BIOELECTRIC PHENOMENA

The application of engineering principles and technology to medicine and biology has had an increasing influence on the practice of medicine. The most visible of these contributions is in the form of medical devices. This article, however, describes the engineering introduction of quantitative methods in the field of bioelectricity. When such contributions first became evident, in the early 1950s many physiology researchers were already employing modern quantitative methods to develop and utilize governing equations and suitable models of bioelectric phenomena. Today it appears that systems physiology lives on as biomedical engineering, while physiology has become more concerned with cell and molecular biology. On the other hand, biomedical engineering is also currently involved in efforts to develop and apply quantitative approaches at cellular and molecular levels.

This article, which is concerned with the electric behavior of tissues, reviews what is known about the biophysics of excitable membranes and the volume conductor in which they are imbedded. Our approach emphasizes the quantitative nature of physical models. We formulate an engineering description of *sources* associated with the propagating action potential and other excitable cellular phenomena. With such sources and a mathematical description of fields generated in a volume conductor the *forward problem,* namely a determination of the potential field at the body surface from underlying bioelectric activity, can be formulated.

The cardiac forward problem starts with a quantitative description of the sources in the heart; the resulting body surface potentials are known as the *electrocardiogram.* In a similar way sources associated with the activation of skeletal muscle lead to the *electromyogram.* We will also consider the *electroencephalogram* and *electrogastrogram,* where we will discover bases for sources other than propagating action potentials. We consider these applications of basic theory only in an introductory way, because there are separate articles for each. It is the goal of this article to elucidate the underlying principles that apply to each of the aforementioned and other applications.

MEMBRANE ELECTROPHYSIOLOGY

Excitable Cells—Macroscopic Structure

The main mammalian tissues that are electrically excitable are nerves and muscles. Although such cells vary greatly in size, shape, and electrical properties, there are nevertheless certain fundamental similarities. In order to illustrate their different cellular structures, we introduce excitable cell histology in this section, although it is somewhat ancillary to the general goals of this article, and it is very brief; the interested reader may consult one of the references for more detailed information. Some additional material will also be found later in this article in the section on "Applications."

Nerve. A sketch of a typical neuron is given in Fig. 1(a), and contains *dendrites,* the *cell body,* and an *axon.* All elements are enclosed by a membrane (which separates the intracellular from the extracellular space) and are electrically excitable. However the axon shown is *myelinated,* that is, its membrane is surrounded by an insulating sheath except at periodic *nodes of Ranvier* (to which any possible transmembrane current is restricted). We are particularly interested in axonal propagation and the accompanying current flow fields. The diameter of nerve fibers varies from 0.3 to 20 μm, (the very small fibers are unmyelinated), and a propagation velocity of 0.5 to 120 m/sec (higher for larger diameters) is observed. One of the main effects of myelination is an increase in propagation velocity for the same fiber diameter. The length of an axon can vary from micrometers (cells in the cortex) to meters (motoneurons from the spinal cord to extremities).

Skeletal Muscle. A description of skeletal muscle structure is given in Fig. 1(b). The whole muscle is shown subdivided into fascicles, each of which contains many fibers. An individual fiber contains *myofibrils,* which constitute the contractile machinery of the muscle. The membrane surrounding each fiber is excitable. Axial propagation of an electrical impulse can take place over this membrane, just as for the nerve axon. However the muscle fiber has a transverse structure namely the *T system,* which is also excitable and which conducts the electrical impulse from the surface radially inward, where it activates the *sarcoplasmic reticulum* (SR); this, in turn, initiates excitation–contraction of the muscle. Because it is unmyelinated, propagation velocity is not as great as for nerve fi-

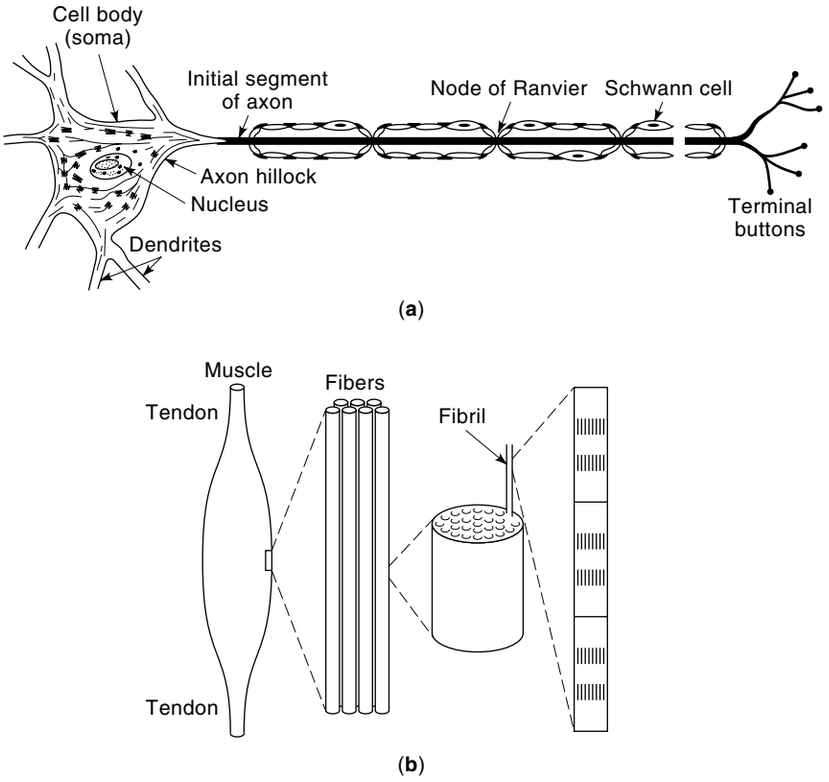

Figure 1. (a) A motor-neuron is shown with typical structure including dendrites, cell body, and axon. Activation of the cell body arises from the summation of excitatory inputs from the dendrites. A propagating impulse travels out on the axon to terminal buttons (neuromuscular junctions) at which the impulse is conducted to a target muscle. The axon shows Schwann cells that provide the myelin sheath, which effectively insulates the axon except at the nodes of Ranvier. From W. F. Ganong *Medical Physiology,* Los Altos, CA: Lange Medical Pub, 1971. (b) The arrangement of fibers in a whole muscle and the myofibrils contained in each fiber. The excitable plasma membrane surrounds each fiber, and the contractile machinery is responsible for the cross-striations seen in each fibril. From Keynes and Aidley, *Nerve and Muscle,* Cambridge: Cambridge University Press, 1981 after K. Schmidt-Nielsen, *Animal Physiology,* Cambridge: Cambridge University Press, 1979.

bers (typically 5 m/sec) and its diameter lies between 10 μm and 100 μm.

When skeletal muscle is viewed under the microscope, characteristic cross-striations are seen. This arises from the arrangement of thin and thick filaments, components of the myofibrils; interaction of the filaments is the basis for the development of contractile force.

Cardiac Muscle. The cardiac muscle fiber looks superficially like that of the skeletal muscle fiber containing, in particular, similar contractile proteins (the T system location differs from that of skeletal muscle) and show the same striation pattern. Cardiac cells, however, do not comprise long fibers, as in skeletal muscle. A typical cardiac cell length is only 100 μm. However cardiac cells are interconnected by gap junctions, which are sites through which ions and hence electric activity may easily pass. Consequently cardiac muscle propagation can take place throughout cardiac tissue as if, functionally, cell membranes were contiguous (*syncytial*).

Smooth Muscle. Smooth muscle differs from skeletal and cardiac muscle in that it does not exhibit cross-striations. It also has a poorly developed SR. There are thick and thin contractile filaments, however their structure is irregular, which accounts for the absence of a banded appearance. Smooth muscle cells range in size from 2 to 10 μm diameter and 20–600 μm length. Individual cells are joined together mechanically by attachment plaques and, often, electrically via gap junctions. This structural arrangement is similar to that found in cardiac muscle. The gap junctions are of low electric resistance and contribute intercellular coupling, which acts to synchronize electrical activity of adjoining cells.

Excitable Cells—Membrane Structure

The simplest electrophysiologic model is that of a single excitable cell lying in an unbounded uniform conducting medium. If we imagine the cell to have been activated, then *action currents* will be observed to flow from the activated site throughout the intracellular and extracellular space. The source of this current is associated with the membrane (since both intracellular and extracellular regions are passive). This section is devoted to a consideration of the structure and function of the biological membrane.

The main constituent of the biological membrane is a lipid bilayer, approximately 5 nm thick, as illustrated in Fig. 2. Because this material is oily, it has a very high electrical resistance and is an effective insulator to ion movement. There are, however, transmembrane proteins that contain aqueous channels; it is only the presence of these channels that endows membranes with ionic permeability.

Channel proteins have been studied biophysically by electron microscopy, electron diffraction, and biologically at the level of molecular structure. Although a fairly consistent picture emerges, we still do not have an accurate structural model. Based on what is known, Hille (1) created the cartoon of a channel protein given in Fig. 2. A typical such protein is approximately 120 Å in length and 80 Å in diameter. Important for ion movement is the aqueous channel. These channels also have *gates,* the opening and closing of which control ion flow. These gates are typically sensitive to electric fields in the membrane, implying that the channel protein contains charged regions that are influenced by the electric field to cause a conformational change, which, in some way, controls the gate. Another important channel property is *selectivity,*

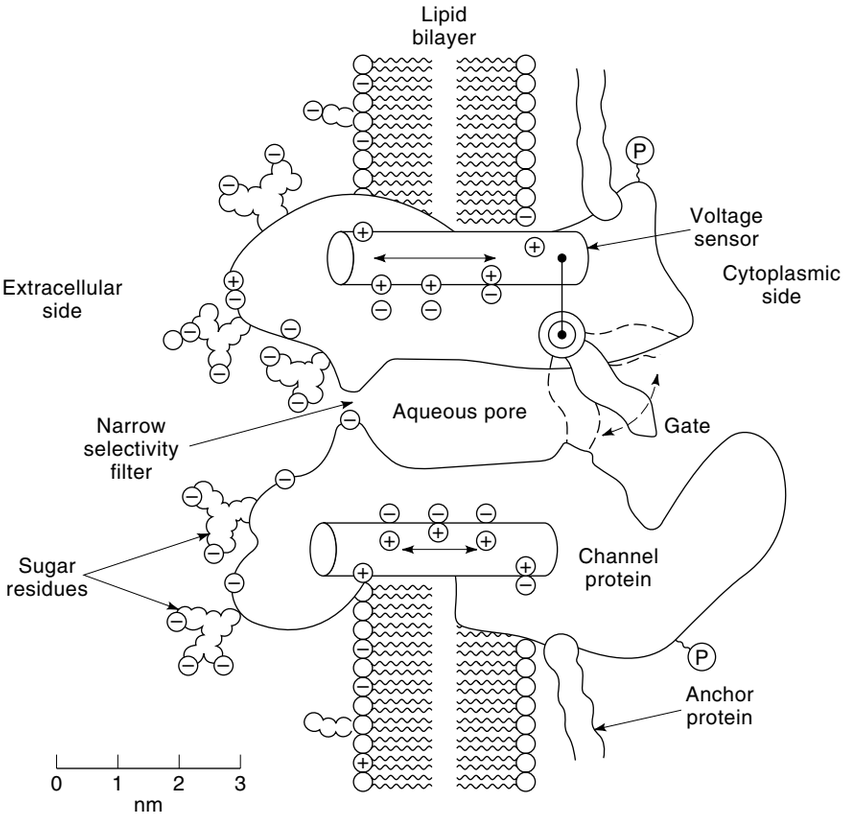

Figure 2. The figure shows the membrane that bounds an excitable cell consisting of a lipid bilayer (two layers of lipid with their hydrophillic heads facing outward and nonpolar tails inward) and an ionic channel that penetrates this layer. The channel structure is based on electron microscopy and electron diffraction studies. "The channel is drawn as a transmembrane macromolecule with a hole through the center. The external surface of the molecule is glycosylated. The functional regions—selectivity filter, gate, and sensor—are deduced from voltage-clamp experiments and are only beginning to be charted by structural studies. We have yet to learn how they actually look." Figure and quotation from B. Hille, *Ionic Channels of Excitable Membranes,* 2nd ed., Sunderland, MA: Sinauer Assoc., 1992.

by which a channel may allow the passage of only one particular ion species; selectivity may depend on the channel diameter, the charges that line the channel, or other details.

An important tool in the study of membranes is molecular genetics. These techniques have been used to determine the primary structure of most channels of interest. Unfortunately it has not been possible to deduce the secondary and tertiary structure. However educated guesses lead to a determination of which portions of the primary amino acid sequence is intramembrane, cytoplasmic, and extracellular. As noted in Fig. 2 the channel protein extends into the cytoplasm as well as the extracellular space.

The Squid Axon

Hodgkin and Huxley (2) pioneered a quantitative study of excitable membranes in the 1950s. For their preparation, they used the giant axon of the squid. This axon was chosen because of its large diameter (approximately 500 μm), which allowed the insertion of an axial electrode. Until this time all measurements of the electric behavior of excitable cells utilized only external electrodes, which left much information inaccessible. In the absence of intracellular potentials the conventional wisdom was that the resting membrane was *depolarized,* meaning that it was at zero transmembrane potential (the term depolarization continues to be used, although it now simply implies activation of an excitable membrane). Hodgkin and Huxley measured resting potentials on the order of -70 mV (inside minus outside).

The squid axon, like any nerve, can be activated by passing an adequate (transthreshold) pulse of current between two electrodes in the external bath. A propagating action potential of the shape described in Fig. 3 is initiated at the activating end and travels to the opposite end. Except for end effects propagation is characterized by an unchanging waveshape and uniform velocity (assuming an axially uniform preparation).

The squid axon exemplifies an unmyelinated nerve fiber. Although this is not typical of nerve fibers in the human body, it presents a very simple model for analysis. One may consider that the intracellular space is simply a uniform electrolyte, whereas the extracellular space (sea water) constitutes an independent electrolyte. Both intracellular and extracellular regions are electrically passive, and consequently whatever mechanism is responsible for the action potential must involve the membrane.

From a chemical analysis of intracellular fluid and sea water (which constitutes the extracellular environment for the squid), Hodgkin and Huxley determined that the major ions available for current flow are K^+, Na^+, and Cl^-. They also noted that the ionic composition of the extracellular fluid differs markedly from the intracellular. The intracellular and extracellular concentrations of the aforementioned ions associated with the squid giant axon are shown in Table 1.

The squid axon contains a very high intracellular potassium concentration. If we assume the membrane to be permeable only to potassium, then from Table 1 we would expect potassium ions to flow out of the intracellular space to the lower concentration extracellular space. This single ion movement can only be transient, because positive charge will accumulate at the outside of the membrane, leaving negative

Table 1. Intracellular and Extracellular Concentrations of Ions Associated with the Squid Giant Axon

Ion	Intracellular (mM)	Extracellular (mM)
K^{+1}	345	10
Na^{+1}	72	455
Cl^{-1}	61	540

Source. Hodgkin-Huxley (2).

charge at the inside surface of the membrane and thereby establishing an electric field that acts inward and inhibits further potassium efflux. (Note that the lipid bilayer constitutes an ideal capacitive dielectric, and a typical membrane capacitance for charge storage is $1\,\mu F/cm^2$). Equilibrium requires that the outward flux due to diffusion be balanced by the inward flux due to the resultant electric field (additional details will be presented shortly). Writing and equating such equations permits the derivation of the *Nernst equation,* which evaluates the single-ion transmembrane potential for an ion to be in equilibrium. For the potassium ion example, it is given as

$$V_m = \frac{RT}{F} \ln \frac{[K_o]}{[K_i]} = 25.2 \ln \frac{[K_o]}{[K_i]} \text{ in mV} \tag{1}$$

where V_m is the transmembrane potential defined as the intracellular minus extracellular potential across the membrane, R is the gas constant, F Faraday's constant, and T the absolute temperature. The coefficient RT/F evaluates to 25.2, for V_m in mV, assuming T at room temperature (20 °C). Note that for anions the ratio in Eq. (1) must be inverted, giving (for chloride) $V_m = 25.2$ ln ($[Cl_i]/[Cl_o]$). For the numerical values in Table 1 we evaluate the potassium Nernst potential as −89.2 mV, the chloride as −54.09 mV, and the sodium as +46.5 mV.

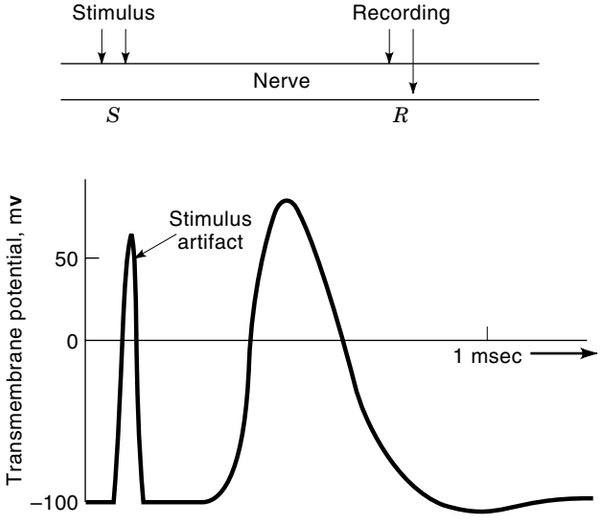

Figure 3. The transmembrane potential measured with an intracellular microelectrode registers the stimulus artifact and an elicited action potential on a nerve axon. The electrode configuration is shown in the inset above. The transmembrane potential does not return to baseline smoothly but shows a positive after-potential.

Even though the resting potassium permeability exceeds that of the chloride and sodium ions, the latter are not negligible. However from the numerical values found previously, it is clear that there is no transmembrane potential that will equilibrate all ions. Consequently the condition that must be met at rest is that of a zero net transmembrane current that is, a *steady-state* condition where

$$I_K + I_{Cl} + I_{Na} = 0 \tag{2}$$

Each ionic current based on diffusion and electric field has been evaluated (3,4). The flux component due to diffusion or the presence of a concentration gradient is described by Fick's law. This gives the ith ion flux as

$$j_{di} = -D_i dC_i/dx \tag{3}$$

where D_i is Fick's constant and x is the direction across the membrane; the flux is from high to low concentration. The flux due to the electric field is given by

$$j_{ei} = -u_i(z_i/|z_i|)C_i \nabla\Phi \tag{4}$$

where u_i is the ion's mobility, z_i it's valence, and $\nabla\Phi$ the potential gradient. Goldman assumed a constant electric field in the membrane and hence set

$$-\nabla\Phi = V_m/d \tag{5}$$

where d is the membrane thickness; the outward electric field is evaluated in Eq. (5).

The electric current is evaluated by multiplying the aforementioned flux (in moles/cm^2) by Faraday's constant, F, times $z_i/|z_i|$ to take account the sign of the ion flow. Thus with $j_i = j_{di} + j_{ei}$ the electric current density, I_i, is

$$I_i = F(z_i/|z_i|)j_i \tag{6}$$

To add Eq. (3) and Eq. (4), a relationship between D_i and u_i is needed; this was furnished by Einstein (5) in the expression

$$D_i = \frac{u_i RT}{|z_i|F} \tag{7}$$

Evaluating the potassium, sodium, and chloride electric currents arising from Eqs. (3), (4), and (7) and inserting each into the steady-state constraint of Eq. (2) leads to the following equation for the steady-state transmembrane potential V_m namely

$$V_m = 25.2 \ln \left(\frac{P_K[K]_o + P_{Na}[Na]_o + P_{Cl}[Cl]_i}{P_K[K]_i + P_{Na}[Na]_i + P_{Cl}[Cl]_o} \right) \tag{8}$$

where RT/F is replaced by 25.2 for $T = 293$ °C and hence V_m is assumed to be in mV (4). In Eq. (8) P_i is the permeability of the ith ion equal to D_i/d in this simple model. Note that, if we assume $P_{Na} = P_{Cl} = 0$, Eq. (8) degenerates into Eq. (1). Hodgkin and Katz (4) applied Eq. (8) to their experiments and found a good fit utilizing $P_K : P_{Na} : P_{Cl} = 1.0 : 0.04 : 0.45$, which yields a value of $V_m = -59.5$ mV. As expected the resting potential does not equilibrate any individual ion, although the

chloride is close to its Nernst potential in this illustration. The sodium ion has a driving force (i.e., there is a difference between the actual transmembrane potential and the value that would result in equilibrium) of $-59.5 - (+ 46.5) = -106$ mV (which, being negative represents a net inward electric field), whereas potassium has a driving force of 29.7 mV [$= -59.5 - (-89.2)$] which, being positive is an outward field. In spite of the much larger sodium driving force its low permeability results in a lower sodium influx than potassium efflux. The excess potassium efflux is balanced by the chloride efflux (driven by the voltage $-59.5 + 54.9 = -4.6$ mV) (where chloride, being negatively charged, moves outward under the net inward electric field) bringing the total current to zero.

Patch Clamp

The Nobel prize-winning work of Neher and Sakmann (6) was for the development of the Patch Electrode. This is a glass micropipette with a tip diameter of 1 μm or less. It is carefully fire-polished so that when placed against a cell membrane and with the application of gentle suction a very high resistance (gigaOhms) seal may be achieved. (Special cleaning of the cell membrane may also be required.) Once this very high resistance seal is achieved, then, as described in Fig. 4, four configurations can subsequently be obtained. In the *cell-attached* configuration the patch electrode measures transmembrane currents over the small membrane area contacted; the cell itself remains intact. Other configurations include only the membrane patch itself or the entire cell membrane (patch removed).

The results of an experiment with the cell-attached electrode are shown in Fig. 5, which gives the transmembrane current response to a transmembrane voltage step; nine successive trials are described. In each case it is seen that in the small accessed area only a single channel (identified as potassium) contributes to the measured current; the current is either zero or 1.5 Pa depending on whether the channel is closed or open. The need for a gigaOhm seal can now be understood as necessary to prevent currents from entering the patch electrode via an extracellular pathway (leakage currents); without the gigaseal even small amounts of such extraneous currents could easily obscure the extremely small desired transmembrane current.

A number of important characteristics of the single channel can be deduced from the experiments shown in Fig. 5. We note that the channel has only two states—either open or closed. From the successive trials we also see that the response is different each time and is hence stochastic. On the other hand when a large number of successive trials are summed we see that a definite pattern emerges, so that the probability, $n(t)$, that a channel is open can be described as a function of time; this is the same function as the averaged channel conductance as a function of time as seen in the ensemble average curve [Fig. 5(b)]. Although this curve can be found by averaging 40 successive trials of the same single channel, we would also expect this result were we to conduct a single trial in which the simultaneous current from 40 channels were measured. In fact in the whole-cell recording configuration (Fig. 4) because both the intracellular and extracellular regions must have the same potential, the entire cell membrane is at the same transmembrane voltage and all channels are in parallel; the measured transmembrane current for a single ion will then be proportional to the probability that a single channel is open.

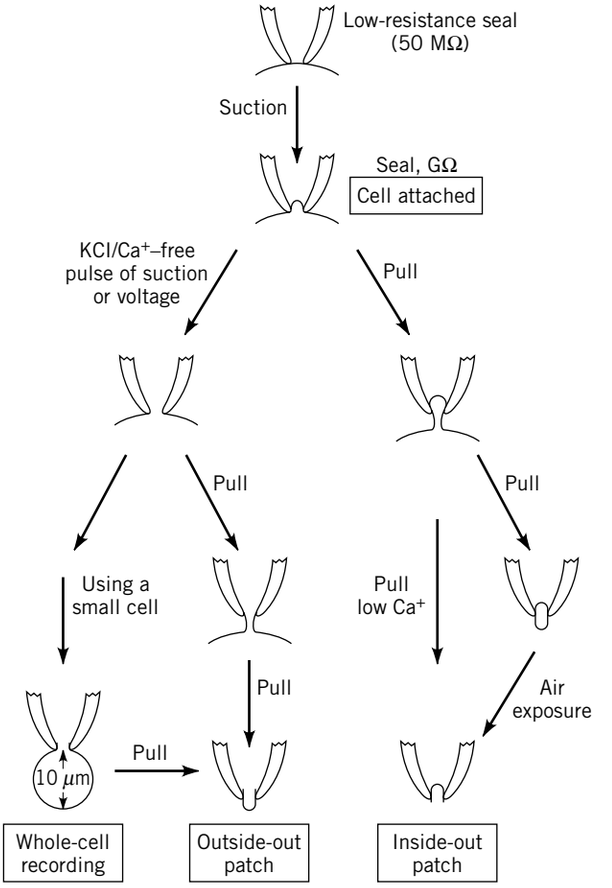

Figure 4. Four configurations for patch clamping are described. The clean pipette is pressed against a cell to form a tight seal using light suction, and producing the *cell-attached* or *on-cell* configuration. Pulling the pipette away from the cell establishes an *inside-out* patch. Application of a suction pulse disrupts the membrane patch, allowing electrical and diffusional access to the cell interior for *whole-cell* recording. Pulling away from the whole-cell arrangement causes the membrane to reform into an *outside-out* configuration. From O. P. Hamill, A. Marty, B. Sakmann, and F. J. Sigworth, Improved patch clamp techniques for high resolution current recording from cells and cell-free membrane patches, *Pflugers Arch.,* **391**: 85–100, 1981.

We also note from Fig. 5 that although the on–off intervals change as a function of time (these are the aforementioned random variables) the magnitude of channel current is fixed. Scaling the curve in Fig. 5 we deduce that the channel conductance is roughly 20 pS. Thus, when the channel is open we can describe its current as

$$i_K = 20(V_m - E_K) \text{ pA} \tag{9}$$

where E_K is the potassium equilibrium (Nernst) potential. Furthermore, assuming a first-order rate process and letting the aforementioned $n(t)$ be the probability of a channel being open we have

$$\frac{dn}{dt} = \alpha(1 - n) - \beta n \tag{10}$$

where β is the probability of a transition from open to closed and α is the probability of a transition from closed to open. Equation (10) describes the time rate of increase in probability of a channel being open as the probabilty of a change from the closed to the open state [namely α times the probability of being closed $(1 - n)$] minus the probability of a change from open back to closed (namely β times the probability of being in the open state n). If the potassium channel density is C channels per square centimeter then the membrane-specific conductance will be $20nC$ pS/cm^2, because nC will be open for a large number of channels.

Hodgkin–Huxley Membrane Model

In developing a practical membrane model one must take into account a very large number of channels of several ion species. A macroscopic model could then be developed, in principle, from single-channel studies. However, to date, membrane models have been formulated from experiments conducted with macroscopic membranes. Illustrative of this approach is the now classical work of Hodgkin and Huxley (2), who constructed the first mathematical model of excitable membrane behavior in the early 1950s. This model was so successful that it continues to be utilized today, although we now have improved models for cardiac tissue and for myelinated nerve.

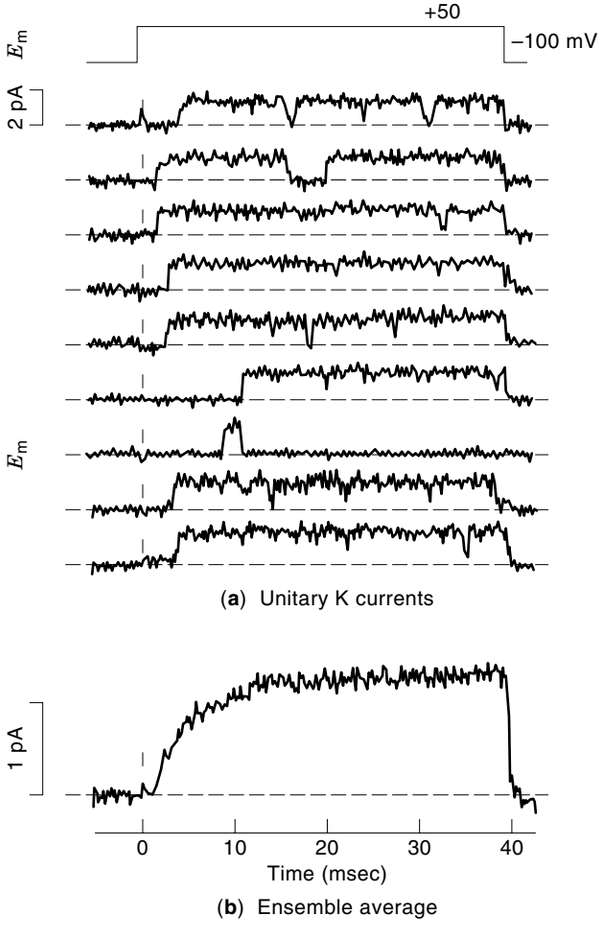

Figure 5. Patch-clamp recording of single-channel potassium currents in a squid giant axon for a voltage clamp of +50 mV. Nine consecutive trials are shown in (a). Based on a driving voltage of +100 mV and an open channel current of 2 pA, a channel conductance of 20 pS results. The recordings are low-pass filtered with a cutoff of 2 kHz. The ensemble mean of 40 trials is given in (b). $T =$ 20 °C. Data provided by F. Bezanilla and C. K. Augustine. Figure from B. Hille, *Ionic Channels of Excitable Membranes.* 2nd ed., Sunderland, MA: Sinauer Assoc., 1992.

In the 1950s electrode sizes were much larger than today. To accommodate a larger electrode, Hodgkin and Huxley chose the giant squid axon as their preparation. This cell has a diameter of approximately 500 μm and was large enough to accommodate an axial electrode. Their second electrode was a concentric cylinder, which was placed in the extracellular electrolyte (sea water). This configuration insured no axial variation in potential so that the entire cell membrane behaved synchronously (i.e., like a large number of membrane patches in parallel). They described this arrangement as *space clamped.* From their studies Hodgkin and Huxley concluded that the transmembrane current was essentially carried by sodium and potassium ions (chloride being at or close to equilibrium). But while a patch electrode is capable of measuring a single ion current, the transmembrane current in the whole axon preparation would necessarily contain both sodium and potassium contributions. To separate these they implemented the *voltage clamp.*

To set the stage for the Hodgkin and Huxley's experiments we first describe the basic model they chose. As we've already noted they assumed that the transmembrane current basically consisted of sodium and potassium. Recognizing the contributions from both electric field and diffusion they assumed the relationships introduced earlier, namely that

Potassium:

$$I_K = g_K(V_m - E_K) \tag{11a}$$

Sodium:

$$I_{Na} = g_{Na}(V_m - E_{Na}) \tag{11b}$$

where the conductivities g_K and g_{Na} were expected to be functions of time and transmembrane potential. In Eq. (11) E_K and E_{Na} are the potassium and sodium equilibrium (Nernst) potentials, the difference from V_m being the net ion driving force. I_K and I_{Na} are "ensemble" current densities per unit area of memberane. To account for a small additional *leakage* current they added

$$I_l = g_l(V_m - E_l) \tag{11c}$$

where g_l is an experimentally determined constant and E_l is chosen so that the total ionic current reduces to zero at rest.

Although Hodgkin and Huxley could only guess at the presence of separate single channels of potassium and sodium, their model is consistent with current understanding. To fit their measurements they assumed that the potassium conductivity satisfied

$$g_K = \bar{g}_K n^4 \tag{12}$$

We may interpret this to describe a functional potassium channel with four subunits, each of which must be open for the channel to be open (hence the probability of an open channel is n^4 if n is the probability of an open subunit). Because n describes a probability, then $0 < n \leq 1$, while $\bar{g}_K$ is the largest

possible value of potassium conductance (all potassium channels open). The temporal behavior of the probability n was assumed to follow Eq. (10) where the rate constants α and β depend solely on V_m.

From their measurements Hodgkin and Huxley learned that sodium showed second-order kinetics. To deal with this they let

$$g_{Na} = \bar{g}_{Na} m^3 h \tag{13}$$

and considered m as an activating gating variable and h an inactivating one where each is governed by the same first-order process described in Eq. (10), namely

$$\frac{dm}{dt} = \alpha_m (1 - m) - \beta_m m \tag{14}$$

$$\frac{dh}{dt} = \alpha_h (1 - h) - \beta_h h \tag{15}$$

In these expressions we have $0 < m \leq 1$ and $0 < h \leq 1$ while the α's and β's depend only on V_m.

With the use of feedback electronics, Hodgkin and Huxley applied a step transmembrane voltage (away from rest) to their space-clamped squid axon. The response to a constant voltage was useful in several ways. For one, the capacitive current, CdV_m/dt was zero (except for a brief transient) and did not confound the measured transmembrane current. Secondly the $n(t)$, $m(t)$, $h(t)$ can be easily obtained from solutions of Eqs. (10), (14), (15) since the α and β coefficients, which are functions of V_m, are constants during a voltage clamp. To illustrate, the measured $g_K(t)$ determines an $n(t)$ from Eq. (12) and, from the solution to Eq. (10), this must have the form

$$n(t) = n_\infty - (n_\infty - n_0) e^{-t/\tau_n} \tag{16}$$

where $n_\infty = \alpha_n/(\alpha_n + \beta_n)$ and $\tau_n = 1/(\alpha_n + \beta_n)$. The initial value of $n = n_0$ is obtained from the n_∞ of the rest period. From a curvefit of $g_K(t)$ for a clamped voltage V_m, $n_\infty(V_m)$ and $\tau_n(V_m)$ are obtained and from these $\alpha(V_m)$, $\beta(V_m)$ are found. Measurements over a range of voltage clamp values of V_m give corresponding values of the gating variables α and β; Hodgkin and Huxley used these sample values to define a continuous function.

It remains only to explain how Hodgkin and Huxley separated their measured transmembrane current into its sodium and potassium components. This was done by running a pair of experiments for each voltage clamp. In the first they used a normal extracellular composition. Then this was repeated with the same value of voltage clamp but using a low-sodium extracellular medium (they replaced 90% of the sodium with choline, because the latter is nonionizing but retains isotonicity). This results in a changed sodium Nernst potential and, hence, driving force. They assumed no other changes and that only the sodium current would change in proportion to its change in driving force. Thus the following two equations were obtained at time t, namely for the first experiment

$$I_m(t) = I_{Na}(t) + I_K(t) \tag{17a}$$

where $I_m(t)$ is the total measured transmembrane current as a function of time, and for the second trial (primed notation)

$$I_m(t)' = I_{Na}(t) \frac{V_m - E'_{Na}}{V_m - E_{Na}} + I_K(t) \tag{17b}$$

Note that $I_K(t)$ and $I_{Na}(t)$ appearing in Eq. (17b) are assumed the same as in Eq. (17a). From these two equations, the two unknown values of $I_{Na}(t)$ and $I_K(t)$ are obtained.

The continuous functional expressions chosen by Hodgkin and Huxley to approximate their discrete measurements of the α's and β's are given below:

$$\alpha_n = \frac{0.01(10 - v_m)}{\exp[(10 - v_m)/10] - 1}, \quad \beta_n = 0.125 \exp\left(\frac{-v_m}{80}\right) \tag{18}$$

$$\alpha_m = \frac{0.1(25 - v_m)}{\exp[(25 - v_m)/10] - 1}, \quad \beta_m = 4 \exp\left(-\frac{v_m}{18}\right) \tag{19}$$

$$\alpha_h = 0.07 \exp\left(-\frac{v_m}{20}\right), \qquad \beta_h = \left\{\exp\left[\frac{(30 - v_m)}{10}\right] + 1\right\}^{-1} \tag{20}$$

In these expressions v_m is the transmembrane potential variation from the resting value, that is $v_m = V_m - V_{rest}$, so that it reflects the true signal apart from a dc component. The numerical values in Eqs. (18) to (20) are based on v_m in millivolts.

The total transmembrane current per unit area is evaluated by summing Eqs. (11a) and (11b) and adding the capacitive component namely $c_m dv_m/dt$ where c_m is the specific capacitance in farads per unit area. The capacitance has already been noted to correspond to the physical membrane structure and is consequently fairly uniform among various membrane types. For the squid axon, and many other membranes, it equals 1.0 μF/cm^2. As might be expected it does not vary with time or transmembrane voltage. A complete expression for membrane current density, i_m, may thus be given as

$$i_m = c_m \frac{dv_m}{dt} + I_K + I_{Na} + I_l \tag{21}$$

The remaining values are needed to implement a Hodgkin–Huxley simulation:

$$\bar{g}_K = 36\ 36\ \text{mS/cm}^2, \quad \bar{g}_{Na} = 120\ \text{mS/cm}^2, \quad \bar{g}_l = 0.3\ 0.3\ \text{mS/cm}^2 \tag{22}$$

Although the system of equations given by Hodgkin and Huxley were derived from voltage-clamped conditions, they successfully describe general temporal behavior very closely. In particular a correct subthreshold and transthreshold response is quantitatively described. Many observed electrophysiological phenomena such as anode break, refractoriness, and so on, are correctly and quantitatively simulated. To implement these equations fast computers and numerical techniques are normally needed. The methodology may be found in one of numerous current references (7,8).

The Hodgkin–Huxley equations describe ionic flow based on the unequal composition of extracellular and intracellular regions; the resulting flux is entirely due to the stored energy associated with the concentration gradient (i.e. a *passive* response). But the membrane also contains a *sodium–potassium pump*. This is an active process that maintains normal composition by transporting sodium out and potassium into the cell. This active transport exactly compensates for the passive flux of sodium into and potassium out of the cell during an action potential and at rest. The pump requires energy to drive ions against their electrochemical gradient

and this is provided by high energy phosphates (ATP). The inclusion of the Na-K pump in our model is important not only to adequately describe axon electrophysiology over a long time interval (when otherwise the system would "run down") but also because the pump exchanges three sodium for two potassium and hence adds to the total transmembrane current (though, on average, usually a relatively small amount). It is nevertheless *electrogenic.*

The Hodgkin–Huxley model has been applied successfully to tissue other than squid axons. For myelinated nerve it is applied at the Nodes of Ranvier, assuming the myelin sheath to insulate the intracellular from extracellular space elsewhere. It has also been used in the simulation of activation of striated muscle. However in both aforementioned applications the modification introduced by Frankenhaeuser (9) is generally more satisfactory. For cardiac muscle the action potential differs from the aforementioned by a very long plateau and slow recovery (each phase lasting for roughly 100 msec). This plays an important functional role in protecting the heart by introducing a long refractory period and hence inhibiting the re-entry of excitation (since activation can be present for perhaps 60 msec). Present day electrophysiological models of the cardiac action potential (10) differ considerably from the simple Hodgkin–Huxley model in that they contain as many as 11 current sources. The unique plateau arises from a delicate balance of component currents which are capable of adapting to changes in the heart rate. These models also include the calcium ion flow; this ion is important since it contributes to maintaining the plateau and also since it triggers the coupling from electrical to mechanical activity of the heart muscle.

Electrical Stimulation

If a very low amplitude pulse of current is passed between the inner and outer electrode of the Hodgkin–Huxley space-clamped preparation the equations describe a membrane response that corresponds to a passive resistance–capacitance (RC) parallel circuit. The membrane resistance is essentially its resting value, which can be found by evaluating n, m, and h when $v_m = 0$ and then introducing this into the expressions for $g_K(0)$, $g_{Na}(0)$, and g_l, whereupon $R_m = A[g_K(0) + g_{Na}(0) + g_l]^{-1}$, where A is the total membrane area in square centimeters. The associated capacitance is simply $C_m = A(1.0)\mu$F. Simple electric circuit theory describes the membrane response to the current pulse, I_0, as

$$v_m = I_0 R_m (1 - e^{t/\tau_m}) \tag{23}$$

where $\tau_m = R_m C_m$ is the membrane time constant.

If the pulse amplitude is increased, a point will be reached where an *action potential* is elicited. This marks the membrane *threshold.* It is frequently assumed that this is a fixed value arising from the intrinsic membrane excitability. Assuming this to be so, then Eq. (23) could be used to find combinations of current strength and duration that would result in an action potential. Thus calling V_T the threshold voltage and using Eq. (23) we have the threshold current as a function of duration, T, namely

$$I_0(T) = I_T (1 - e^{-T/\tau_m})^{-1} \tag{24}$$

where $I_T = V_T/R_m$ is the threshold current amplitude for $T \to \infty$. Equation (24) is called the *strength–duration* curve and is seen to have a characteristic hyperbolic shape. For $T \to \infty$ we note that the minimum stimulus amplitude is found (namely $I_T = V_T/R_m$), and this is described as the *rheobase*. For a stimulus of twice rheobase the duration, according to Eq. (24), is $T_c = 0.6931\tau_m$ where T_c is referred to as the *chronaxie.*

An experimental determination of the strength–duration curve can be performed on the space-clamped squid axon, as described above. A similar experiment can be performed by simulation using the above Hodgkin–Huxley equations. In either case the outcome will be similar and can also be interpreted as describing the behavior of a membrane patch. One can verify that the assumption of a constant threshold is supported provided the duration satisfies $0.05 < T < 5$ msec hence validating Eq. (24) for this condition (a threshold of approximately 8 mV is found). Outside this range other factors enter the functional threshold. For very small durations the membrane needs to be brought to higher threshold voltages, so that following termination of the stimulus, as the membrane charge leaks away and the voltage diminishes, an adequate transmembrane potential remains to continue the process of opening sodium gates (the time constant for m is in tenths of a millisecond). For long-duration stimulii membrane inactivation, reflected in diminishing values of h, needs to be overcome with higher effective thresholds.

The above limitations regarding threshold apply only to the membrane patch. However, electrical stimulation of interest normally involves extracellular electrodes placed near or in extensive tissue membranes. In this case depolarizing voltages are also accompanied by hyperpolarizing voltages, both of which may be distributed over a complicated geometry. Interestingly, even in such circumstances, experimentally determined strength–duration curves are still seen to follow a behavior not too different from Eq. (24). In fact a better fit often arises with a simpler form of Eq. (24), obtained by approximating $(1 - e^{-T/\tau})^{-1} \approx \tau_m/T$ valid for small T. This approximation can be made to hold also for large T by taking $(1 - e^{-T/\tau})^{-1} \approx 1 + \tau_m/T$ giving

$$\frac{I_0(T)}{I_T} = 1 + \frac{\tau_m}{T} \tag{25}$$

Equation (25) is known as the Weiss–Lapique formula. Multiplying Eq. (25) by T and describing $Q_T = I_0(T)T$ as the threshold charge results in

$$Q_T = I_T(T + \tau_m) \tag{26}$$

which predicts a linear relationship with duration for the threshold charge Q_T. This is, in fact, frequently seen; the value of τ_m is determined experimentally by curve-fitting strength–duration measurements and is surprisingly found to approximate the membrane time constant.

SOURCE-FIELD RELATIONSHIPS

In electrocardiography, electromyography, and so on, electrical signals originating in a specific excitable tissue is measured with extracellular electrodes. In fact the usual case is that electrodes lie at the body surface (i.e., so that measurements are noninvasive) in which case a clear separation ex-

ists between the excitable tissues and the recording electrode(s). To simulate this situation quantitatively there are two main considerations. The first is to find an engineering (quantitative) description of the sources that are generated by tissue activation. The second, based on such a source description, is to evaluate the currents that will flow in the surrounding passive volume conductor. One is particularly interested in the associated electrical potential field, which will be sampled by the recording electrodes. These two goals are the subject of this section.

Example—Long Fiber in an Unbounded Volume Conductor

We begin by considering an excitable, infinitely long fiber lying in an unbounded volume conductor. This idealized model could approximate a long skeletal muscle or squid axon fiber in a volume conductor whose extent is large compared to fiber dimensions (we'll be more precise about this later). We assume that a propagating action potential has been initiated, so that at the moment a full spatial action potential $v_m(z)$ is present on the fiber. Since fibers are very long compared to their small diameter we may assume no intracellular radial variation of current density or potential and consequently that we can describe $\Phi_i(z)$ as the intracellular potential, a function only of the axial coordinate, z. Ohm's law links the total intracellular axial current, $I_i(z)$, with the intracellular field, $\partial\Phi_i(z)/\partial z$, according to

$$-\frac{\partial \Phi_i(z)}{\partial z} = I_i r_i \tag{27}$$

where r_i is the intracellular resistance per unit length. (The intracellular resistance per unit length, r_i, can be evaluated from the intracellular resistivity, ρ_i, and the fiber radius a, using $r_i = \rho_i/(\pi a^2)$.) Continuity requires that whatever current is lost from the intracellular space appear as an outward transmembrane current and consequently

$$i_m = -\frac{\partial I_i}{\partial z} \tag{28}$$

where i_m is the transmembrane current per unit length. Combining Eqs. (27) and (28) gives the classical linear-core-conductor expression namely

$$i_m(z) = \frac{1}{r_i}\frac{\partial^2 \Phi_i(z)}{\partial z^2} \tag{29}$$

The starting point for Hodgkin–Huxley simulation of a propagating action potential is equating Eq. (29) with Eq. (21).

Since physiological fibers are very long compared to their diameters, then for points in the volume conductor that are well outside the fiber we can consider the transmembrane current to arise from a line source on the fiber axis. A short fiber element of length dz will behave like a point source of current ($i_m dz$). Again, because fibers are normally very thin, the fiber's presence within the volume conductor may be ignored, and we may consider the current from the aforementioned element to flow into an unbounded conductor. Now the current density from a point current source, I_0, through a concentric sphere of radius R, where all lie in a uniform, unbounded conductor, is by symmetry simply $I_0/(4\pi R^2)$. The electric field at that point, $-\partial\Phi_e/\partial R$, from Ohm's law is $I_0/(4\pi\sigma_e R^2)$ where the extracellular medium has a uniform conductivity of σ_e. Integrating with respect to R gives the potential field generated by a point source as

$$\begin{aligned}\Phi_e &= I_0/(4\pi\sigma_e R)\\ &= i_m\, dz/(4\pi\sigma_e R)\end{aligned} \tag{30}$$

where we replaced I_0 by the point source element $i_m dz$. Substituting Eq. (29) into Eq. (30) and integrating over z gives an expression for the field of a fiber lying in an unbounded uniform volume conductor and which is carrying an action potential as

$$\Phi_e = \frac{a^2\sigma_i}{4\sigma_e}\int \frac{\partial^2 v_m}{\partial z^2}\frac{1}{R}\,dz \tag{31}$$

where $r_i = (\pi a^2\sigma_i)^{-1}$. In Eq. (31) we replaced Φ_i by v_m since for an unbounded volume conductor, in view of the extensive short-circuiting, $\Phi_e \approx 0$, and consequently $v_m = \Phi_i - \Phi_e \approx \Phi_i$.

In the above source-field considerations the finite fiber radius has been neglected, an approximation that is reflected in the one-dimensional integral in Eq. (31). We may anticipate that quite close to the fiber it may be necessary to take into account that the current is not emerging from an axial source but from a finite cylindrical surface. In addition, each current source element on the membrane surface does not actually see an unbounded medium but rather one in which the fiber itself is embedded. Later on we will obtain a rigorous solution from which this approximate one can be examined.

In the derivation of Eq. (31) we assumed a steady current source and that the electric field can be obtained as the gradient of a scalar potential function, that is, $\boldsymbol{E} = -\nabla\Phi$, which also arises from static considerations. Since biological sources of interest are normally time-varying the aforementioned procedure is open to question. However, it has been shown that for signals of physiologic origin *quasistatic* conditions are in effect (11) and these validate the aforementioned expressions.

Fundamental Source-Field Concepts

Equation (31) illustrates the fundamental concept of *source-field* relationship for a simple preparation, but, in fact, this also applies conceptually to distributed sources in multicellular tissues (heart, brain, muscle, etc.) which generate electrical fields in bounded nonuniform volume conductors (the human body). In Eq. (31), behaving like a point current source is the quantity $i_{source}dz$, where

$$i_{source} = \pi a^2\sigma_i\frac{\partial^2 v_m}{\partial z^2} \tag{32}$$

The line source density, i_{source}, is thereby identified as a *current source* being generated by the propagating action potential $v_m(z)$. The relationship of i_{source} and v_m is specified by Eq. (32) describing the source quantitatively. In turn i_{source} will generate an electric field in the surrounding volume conductor, and this is given by Eq. (31). The total field at any point arises from a summation of contributions from every source element $I_{source}dz$.

To more clearly distinguish source points from field points, since the same coordinate system is being utilized for both, we choose here unprimed coordinates to describe the source and primed coordinates for the field. We may therefore write

Eq. (31) as

$$\Phi_e(x', y', z') = \frac{1}{4\pi\sigma_e} \int \frac{i_{source}(x, y, z)}{\sqrt{(x-x')^2 + (y-y')^2 + (z-z')^2}} dz \tag{33}$$

where we have written out

$$R = \sqrt{(x-x')^2 + (y-y')^2 + (z-z')^2}$$

While an extension of Eq. (32) to include multicellular tissues must still be considered, it seems reasonable to expect that an expression similar to Eq. (32) will arise except that the source needs to be described more generally as a volume source, I_v, in which case i_{source} is a degenerate case when the source can be considered to be one-dimensional. For a volume source Eq. (33) generalizes to

$$\Phi(x', y', z') = \frac{1}{4\pi\sigma} \int \frac{I_v(x, y, z)}{\sqrt{(x-x')^2 + (y-y')^2 + (z-z')^2}} dv \tag{34}$$

where I_v is a volume source density. In the literature I_v is also referred to as an *applied* or an *impressed* source.

An important feature of the field $\Phi(x', y', z')$ can be found by evaluating its Laplacian, which can be accomplished by taking the Laplacian of both sides of Eq. (34). The Laplacian operates at the field point [i.e., with respect to the primed coordinates on the left-hand side of Eq. (34)], so on the right-hand side of Eq. (34) the operator can be taken under the integral sign because the latter is with respect to the unprimed coordinates. In fact, in the integrand of Eq. (34) only R is a function of the primed coordinates, and one can show that $\nabla'^2(1/R) = -4\pi\delta_v$ where δ_v is a unit (volume) *delta function.* Consequently (we now drop the prime notation)

$$\nabla^2\Phi = -\frac{I_v}{\sigma} \tag{35}$$

which is *Poisson's equation.* Even though we understand how to obtain i_{source} for a long, isolated fiber [namely by applying Eq. (32)], we await subsequent material that describes the evaluation of I_v for multicellular preparations. One can also confirm that Eq. (34) does, indeed, apply.

Surface Sources and Field Discontinuities

The field from surface sources have useful properties, which, as we will see, correspond to the fields arising from excitable cells and from volume conductor inhomogeneities. This subsection is consequently devoted to a description of surface-source fields; their application will be given subsequently.

The field of a point source is described by Eq. (30). For a surface source described by $K_S(S)$mA/cm^2, then $K_S(S)\,dS$ constitutes a point source and application of Eq. (30) gives

$$\Phi_S = \frac{1}{4\pi\sigma} \int \frac{K_S(S)}{R} dS \tag{36}$$

Since a surface source occupies zero volume, the Φ_S obtained from Eq. (36) should satisfy Laplace's equation everywhere. But in a completely source-free universe Φ would necessarily be zero everywhere. In what way does the behavior of Φ_S differ (surely it cannot be zero everywhere since there is a source)? We would find that, while Φ_S and its derivatives are well behaved and, in fact, satisfy Laplace's equation everywhere, either Φ_S or its derivative behaves discontinuously in crossing the source surface (the discontinuity depending on the type of surface source).

One way of investigating the behavior of Φ_S is to evaluate it as we proceed along a path that crosses K_S at right angles, as shown in Fig. 6. To facilitate the calculation, we have removed a very small circular disc from the source, where the center of the disc is the point of intersection of the arbitrary path across the source surface, as is also described in Fig. 6. Now in the absence of the disc the integral in Eq. (36) is well behaved everywhere (since $R \neq 0$ everywhere), and both Φ_S and its derivatives are also necessarily well-behaved because there are no singularities. It only remains to investigate the contribution to Φ_S from the circular disc. This disc is so small that we may take it to be planar. If we choose the z axis to lie on the disc axis with its origin at the disc, then the radial cylindrical coordinate ρ lies in the plane of the disc. Application of Eq. (36) gives

$$\begin{aligned} \Phi_S(z) &= \frac{K_S(0)}{4\pi\sigma} \int_0^a \frac{2\pi\rho}{\sqrt{\rho^2 + z^2}} d\rho \\ &= \frac{K_S(0)}{2\sigma} (\sqrt{a^2 + z^2} - |z|) \end{aligned} \tag{37}$$

where $K_S(0)$ is the value of the surface-source density at the disc origin and a is the disc radius. From an examination of Eq. (37), we conclude that Φ_S is continuous across the source surface; however $\partial\Phi_S(z)/\partial z$ is discontinuous. Specifically, from

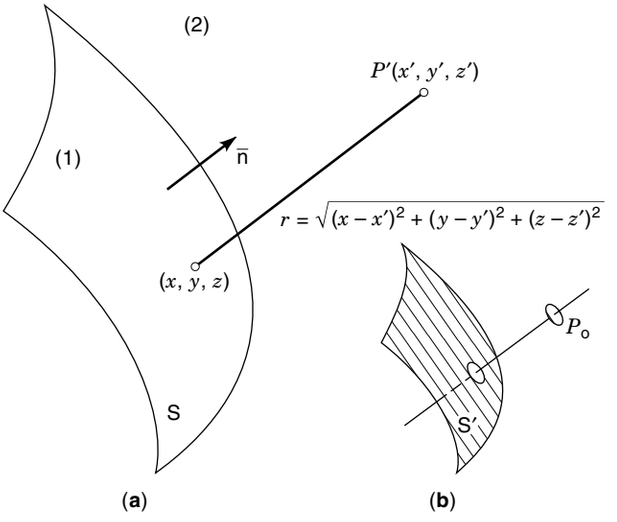

Figure 6. (a) A surface source K_S or double-layer τ lies in the arbitrary surface S. The two sides are denoted 1 and 2 and the positive normal $\boldsymbol{n}$ is from 1 to 2. P' is an arbitrary field point. (b) The behavior of the field at P_0 is examined by decomposition of S into a small source disc centered at P_0 and the remaining sources. The field of the latter are well behaved at P_0 and hence whatever discontinuities might be present can be studied by examining the behavior of the disc field alone. From R. Plonsey, The formulation of bioelectric source-field relationships in terms of surface discontinuities. *J. Franklin Inst.,* **297**: 317–324, 1974.

Eq. (37) we get

$$\Phi_1 = \Phi_2$$
$$\left.\frac{\partial \Phi}{\partial z}\right|_1 - \left.\frac{\partial \Phi}{\partial z}\right|_2 = \frac{K_S}{\sigma} \tag{38}$$

where positive z is directed from 1 to 2.

This result could have been anticipated based on a physical argument. The current source gives rise to a current flow in opposite directions from the source surface. The potential must therefore rise to a peak value at the surface and diminish in both directions away from the sheet to give this expected gradient. So, a continuity of potential results; but, because the derivative of potential is oppositely directed, it is discontinuous. We learn from Eq. (38) that the magnitude of the discontinuity in the normal derivative equals the strength of the surface source (divided by the conductivity) at that point. This is an important equivalence that we subsequently utilize.

A second surface source also must be introduced, which consists of a sheet of dipoles. As a brief review, the dipole consists of two point sources of equal magnitude but opposite sign, which are displaced a very short distance $d\boldsymbol{l}$. If $d\boldsymbol{l} = 0$, the fields of each source combine and cancel. Then we may consider the dipole to be created by displacing the positive source by the small displacement $d\boldsymbol{l}$. The two fields no longer cancel precisely by the change in the field from the positive source. Applying Eq. (30) we have

$$\Phi_{\text{dipole}} = \frac{I_0}{4\pi\sigma}\frac{\partial(1/R)}{\partial l} \tag{39}$$

The partial derivative in Eq. (39) is known as a *directional derivative* and can be found using the gradient operator as

$$\Phi_{\text{dipole}} = \frac{I_0}{4\pi\sigma}\nabla(1/R)\cdot d\boldsymbol{l} \tag{40}$$

In spherical coordinates $\nabla(1/R) = \boldsymbol{a}_R/R^2$ where $\boldsymbol{a}_R$ is a unit vector from the source to the field. Equation (40) may now be written

$$\Phi_{\text{dipole}} = \frac{\boldsymbol{a}_R \cdot \boldsymbol{p}}{4\pi\sigma R^2} \tag{41}$$

where $\boldsymbol{p} = I_0 d\boldsymbol{l}$ is the *dipole moment* (namely the product of monopole strength, I_0, and separation dl in the direction $d\boldsymbol{l}/dl = \boldsymbol{a}_l$.

A surface of dipoles is known as a *double layer*. If we assume such a source surface having a strength $\boldsymbol{\tau}$ (dipole moment per unit area), then $\boldsymbol{\tau} dS$ constitutes a dipole element. As with the single layer its fields are well behaved everywhere except in crossing the source surface. Also, as before, the discontinuity can be examined by considering the field behavior along the axis of a very small double-layer disc. In place of Eq. (36) we now have

$$\Phi_D = \frac{1}{4\pi\sigma}\int \frac{\tau \boldsymbol{a}_R \cdot d\boldsymbol{S}}{R^2} \tag{42}$$

where we use $\boldsymbol{\tau} dS \equiv \tau d\boldsymbol{S}$ because the dipole orientation for a double layer is everywhere normal to the surface. In place of Eq. (37) we now have

$$\Phi_D(z) = \frac{\tau(0)}{4\pi\sigma}\int_0^a \frac{2\pi\rho z\, d\rho}{(\rho^2 + z^2)^{3/2}} \tag{43}$$

where we utilized $\boldsymbol{a}_R \cdot \boldsymbol{a}_z = z/\sqrt{\rho^2 + z^2}$ because the axis of the disc is z. We note from Eq. (43) that the potential is antisymmetric on z. However the normal derivative is an even function of z and is continuous across the disc (across the surface). By evaluating Eq. (43) we can confirm that

$$\Phi_D|_2 - \Phi_D|_1 = \frac{\tau}{\sigma}$$
$$\left.\frac{\partial \Phi_D}{\partial n}\right|_1 = \left.\frac{\partial \Phi_D}{\partial n}\right|_2 \tag{44}$$

The vector double-layer strength is $\boldsymbol{\tau} = \tau \boldsymbol{n}$ where $\boldsymbol{n}$ is the unit surface normal from 1 to 2.

Single Cell Sources

An arbitrary shaped single cell lying in an unbounded volume conductor is described in Fig. 7. The intracellular conductivity is σ_i and the extracellular conductivity σ_e. We assume that an action potential has been initiated at a membrane site and that it is propagating distally eventually to reach all points on the cell surface. The transmembrane potential is consequently a function of position on the cell surface $v_m(S)$ (a two-dimensional function); and this is a more general condition compared with the one-dimensional single-fiber case considered earlier.

Because the membrane is extremely thin compared to all other dimensions of interest we consider it as an interface between the intracellular space [whose potential is designated $\Phi_i(S)$] and the extracellular space [where $\Phi_e(S)$ designates the potential]. We let Φ be the potential field generated by the action potential in either space and define a new scalar potential function Ψ namely

$$\Psi = \Phi\sigma \tag{45}$$

Now Φ satisfies Laplace's equation everywhere, because, except for the membrane that we assume to occupy zero volume, all space is source-free and passive (i.e., there are no volume sources). Consequently, since σ is piecewise constant

$$\nabla^2\Psi = \sigma\nabla^2\Phi = 0 \tag{46}$$

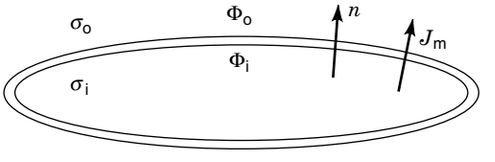

Figure 7. The single cell lies in an unbounded volume conductor. The positive surface normal and transmembrane current is outward. In the figure the transmembrane potential v_m equals the intracellular membrane potential, Φ_i, minus the extracellular membrane potential, Φ_o. The intracellular conductivity is σ_i and the extracellular is σ_o.

and Ψ also satisfies Laplace's equation. From Eq. (35), we note that in the general case

$$\nabla^2\Psi = -I_v \tag{47}$$

so that the solution for Ψ from I_v has the interesting property that it does not depend on the conductivity (although I_v, or a degenerate surface or point source, may so depend). For the single active cell Ψ satisfies the following boundary conditions in crossing the membrane

$$\Psi_\mathrm{i}\big|_\mathrm{S} - \Psi_\mathrm{e}\big|_\mathrm{S} = \sigma_\mathrm{i}\Phi_\mathrm{i}\big|_\mathrm{S} - \sigma_\mathrm{e}\Phi_\mathrm{e}\big|_\mathrm{S} \neq 0 \tag{48}$$

an inequality that reflects both the nonzero transmembrane potential and difference in intracellular–extracellular conductivity. [Note that while the difference in Eq. (48) might be zero at some points it is not identically zero.] A second boundary condition follows from the continuity of current across the membrane. This gives

$$\sigma_\mathrm{i}\left.\frac{\partial\Phi_\mathrm{i}}{\partial n}\right|_\mathrm{S} - \sigma_\mathrm{e}\left.\frac{\partial\Phi_\mathrm{e}}{\partial n}\right|_\mathrm{S} = \left.\frac{\partial\Psi_\mathrm{i}}{\partial n}\right|_\mathrm{S} - \left.\frac{\partial\Psi_\mathrm{e}}{\partial n}\right|_\mathrm{S} = 0 \tag{49}$$

The notation in Eqs. (48) and (49) emphasizes that the Ψ and its normal derivative are evaluated at the membrane surface; n is the outward membrane normal.

An examination of Eqs. (48) and (49) shows that the scalar function Ψ, which satisfies Laplace's equation, has a continuous normal derivative across the membrane, but the function itself is discontinuous. A comparison with Eq. (44) reveals that the membrane behaves like a double layer, lying in the membrane surface, whose strength is

$$\tau = \sigma\Phi^D\big|_2 - \sigma\Phi^D\big|_1 = \Psi_\mathrm{e} - \Psi_\mathrm{i} \tag{50}$$

a result that is obtained by associating region 1 in Fig. 7 with the intracellular, whereas region 2 corresponds to extracellular. Based on Eq. (41)

$$\sigma\Phi = \Psi = \frac{1}{4\pi}\int\frac{\tau\boldsymbol{a}_R\cdot d\boldsymbol{S}}{R^2} \tag{51}$$

and substituting Eq. (50) results in

$$\Psi = \frac{1}{4\pi}\int(\Psi_e - \Psi_i)\frac{\boldsymbol{a}_R\cdot d\boldsymbol{S}}{R^2} \tag{52}$$

As noted earlier we see that the conductivity is absent from the source-field expression for the scalar function Ψ; its source-field relationships appear as if the medium were uniform and homogeneous [but, of course, the discontinuity in conductivity at the membrane interface influences the source strength $\tau = \Psi_\mathrm{e} - \Psi_\mathrm{i}$ according to Eq. (50)]. By applying Eq. (45) to Eq. (52) the desired result is obtained, namely

$$\Phi_p = \frac{1}{4\pi\sigma_p}\int_S(\sigma_\mathrm{e}\Phi_\mathrm{e} - \sigma_\mathrm{i}\Phi_\mathrm{i})\frac{\boldsymbol{a}_R\cdot d\boldsymbol{S}}{R^2} \tag{53}$$

In Eq. (53) we designated the field point with the subscript p so that if it is intracellular (or extracellular) we substitute $\sigma_\mathrm{i}(\sigma_\mathrm{e})$. Although we obtained Eq. (53) by ignoring the finite thickness of a membrane, it can be shown that for biological membranes if its resistivity (which is high) and thickness (which is very small) is taken into account the result given by Eq. (53) is, nevertheless, unchanged. Thus, for a multicellular preparation consisting of cells of arbitrary shape, there will be a double-layer source lying in each cell membrane whose strength and orientation is given by

$$\tau = (\sigma_\mathrm{e}\Phi_\mathrm{e} - \sigma_\mathrm{i}\Phi_\mathrm{i})\boldsymbol{n} \tag{54}$$

where $\boldsymbol{n}$ is the outward unit vector normal to the cell. We designate these sources to be *secondary sources.* This is because a true *primary source* should be directly associated with a source of energy. Here, we note that in Eq. (54) the source strength depends significantly on the discontinuity in conductivity. We show in the following that a source does arise at conductivity discontinuities, but in view of its passive nature must be secondary. A detailed analysis can be found in Plonsey (12). What is important, here, is that a rigorous equivalent source description is that of a distribution of surface double layers.

Inhomogeneous Media—Secondary Sources

Any actual volume conductor normally contains several tissues and hence will be necessarily inhomogeneous. A first approximation is to consider each tissue or organ to be uniform, so that the volume conductor has a conductivity that is piecewise constant. The boundary conditions at the interface between any two regions of different conductivity is based on the continuity of potential and the continuity of current flow normal to the interface. This is written as

$$\begin{aligned}\Phi_1 &= \Phi_2\\ \sigma_1\partial\Phi/\partial n\big|_1 &= \sigma_2\partial\Phi/\partial n\big|_2\end{aligned} \tag{55}$$

The function Ψ, defined in Eq. (45), then satisfies the following boundary conditions

$$\begin{aligned}\Psi_2 - \Psi_1 &= \Phi(\sigma_2 - \sigma_1) \neq 0\\ \partial\Psi/\partial n\big|_2 - \partial\Psi/\partial n\big|_1 &= 0\end{aligned} \tag{56}$$

where we designate $\Phi_1 = \Phi_2 = \Phi$ at the interface [applying Eq. (55)]. As shown above, Ψ satisfies Laplace's equation; its continuous normal derivative and discontinuous function at the boundary can be considered to arise from a double layer at the interface. The strength of the double layer is given by the discontinuity in Ψ at the interface, which, from Eqs. (44) and (56) amounts to

$$\tau = (\sigma_2 - \sigma_1)\Phi\big|_\mathrm{S}\boldsymbol{n} \tag{57}$$

where $\boldsymbol{n}$ is the normal vector from side 1 to 2. This source meets the criteria to be a secondary source, because it comes into existence only when a field is first generated by a primary source. In a volume conductor the presence of an electric field gives rise to conduction currents whose Joule heating necessitates the continual influx of energy to maintain the quasistatic system. This expenditure of energy comes from the primary fields, which can be recognized by their coupling to energy sources such as ATP. (An example is the membrane ion pumps, which maintain the ion composition responsible for membrane ion flow and hence identify the latter as a primary current source.)

In principle we can apply this treatment to a complex inhomogeneous volume conductor. Along each interface between regions of different conductivity Eq. (57) is used. The inhomogeneous volume conductor is, in this way, replaced by a uniform homogeneous medium for the scalar function Ψ [as discussed in connection with Eq. (47)] except that at all interfaces a double layer of the form given in Eq. (57) exists. Clearly the result is a scalar function, Ψ, satisfying Laplace's equation and all boundary conditions [in view of Eq. (44)]; the resultant Ψ is necessarily the correct solution. Assuming multiple cells and an inhomogeneous medium the previous results can be summarized as

$$\Psi = \frac{1}{4\pi}\sum_i \oint_{\text{cells}} (\Psi_e - \Psi_i)\frac{\boldsymbol{a}_R \cdot d\boldsymbol{S}}{R^2} + \frac{1}{4\pi}\sum_j \int_{S_j} \Psi_2 - \Psi_1 \frac{\boldsymbol{a}_R \cdot d\boldsymbol{S}}{R^2} \tag{58}$$

where i enumerates all cells and j all interfacial surfaces. Using Eq. (45) and solving for the potential Φ at the point p results in

$$\begin{aligned}\Phi_p = {} & \frac{1}{4\pi\sigma_p}\sum_i \oint_{\text{cells}} (\sigma_e\Phi_e - \sigma_i\Phi_i)\frac{\boldsymbol{a}_R \cdot d\boldsymbol{S}}{R^2} \\ & + \frac{1}{4\pi\sigma_p}\sum_j \int_{S_j} \Phi(\sigma_j'' - \sigma_j')\frac{\boldsymbol{a}_R \cdot d\boldsymbol{S}}{R^2}\end{aligned} \tag{59}$$

where the conductivity in region 1 is designated with a prime, in region 2 with a double prime, and σ_p designates the conductivity at the field point p.

Long Cylindrical Fiber—Equivalent Sources

In our earlier treatment of the field generated by a single active fiber in an unbounded conductor, approximations were made that limited the result to extracellular field points sufficiently far from the fiber to justify the assumption that the sources be considered localized on the axis. But, now, we have in Eq. (53) an expression that is valid for all field points. This section is devoted to the application of Eq. (53) to the earlier long-fiber geometry. One goal is to quantitatively examine the approximations that lead to Eq. (31). But, in the process, we shall also arrive at other source-field formulations that are mathematically equivalent but have different, possibly useful, physical interpretations. Although all this may seem like too great an effort to devote to one particular geometry, in fact much excitable tissue consists of fibers or, as in the case of cardiac tissue, may be treated as consisting of fibers.

We begin with the single cylindrical fiber as described earlier, where, as before, potentials at the fiber surface depend only on z (i.e., axial symmetry is assumed). If we let

$$-\sigma_i V_f(z) = \sigma_e\Phi_e(z) - \sigma_i\Phi_i(z) \tag{60}$$

where $\Phi_e(z)$ and $\Phi_i(z)$ are extracellular and intracellular potentials at the membrane interface, then, using Eq. (53) we have

$$\Phi(p) = -\frac{1}{4\pi}\frac{\sigma_i}{\sigma_p}\int_S V_f(z)\nabla\left(\frac{1}{R}\right)\cdot d\boldsymbol{S} \tag{61}$$

In Eq. (61) we've replaced $\boldsymbol{a}_R/R^2$ by $\nabla(1/R)$, where $\boldsymbol{a}_R$ is from source to field, consistent with ∇ operating on unprimed, source coordinates (for simplicity in notation we now assign unprimed coordinates to the source). Now we extend our definition of V_f to

$$V_f(\rho, z) = V_f(a, z) = V_f(z) \tag{62}$$

(where a is the fiber radius), so that whereas Eq. (60) limits $V_f(z)$ to the membrane surface [because the right-hand side of Eq. (60) is defined only at that surface], in Eq. (62) this function is defined throughout the fiber volume, although it retains its assigned value at the membrane surface. Consequently this new definition can be given to V_f in Eq. (61), because the surface integral retrieves $V_f(z)$ from $V_f(\rho, z)$ from Eq. (62) and is hence unchanged. But now Gauss's theorem can be applied, converting the surface integral into a volume integral (throughout the fiber volume) which is

$$\Phi(p) = -\frac{1}{4\pi}\frac{\sigma_i}{\sigma_p}\int_V \nabla\cdot\left[V_f(\rho, z)\nabla\left(\frac{1}{R}\right)\right] dv \tag{63}$$

Since V_f now participates in the volume integration, it is clear that its definition within the volume [e.g., Eq. (62)] is required. If the vector identity $\nabla\cdot(\phi\boldsymbol{A}) = \nabla\phi\cdot\boldsymbol{A} + \phi\nabla\cdot\boldsymbol{A}$ is applied to the integrand in Eq. (63), one obtains

$$\nabla\cdot\left[V_f(\rho, z)\nabla\left(\frac{1}{R}\right)\right] = \frac{\partial V_f(z)}{\partial z}\boldsymbol{a}_z\cdot\nabla\left(\frac{1}{R}\right) + V_f(z)\nabla^2\left(\frac{1}{R}\right) \tag{64}$$

where we recognized that $V_f(\rho, z)$ is a function only of z and furthermore that it equals $V_f(z)$. We have commented earlier [see Eq. (35)] that the Laplacian of $1/R$ is a delta function. For exterior field points $R \neq 0$ and the Laplacian is zero. Because our emphasis here is on extracellular fields generated by cellular sources, this will always characterize our situation. Accordingly Eq. (63) can be written

$$\Phi(p) = -\frac{1}{4\pi}\frac{\sigma_i}{\sigma_p}\int_V \frac{\partial V_f(z)}{\partial z}\boldsymbol{a}_z\cdot\nabla\left(\frac{1}{R}\right) dv \tag{65}$$

Incorporating Eq. (60) into Eq. (65) gives

$$\Phi_e(p) = \frac{1}{4\pi\sigma_e}\int_z \frac{\partial[\sigma_e\Phi_e(z) - \sigma_i\Phi_i(z)]}{\partial z}dz\int_A \frac{\partial(1/R)}{\partial z}dA \tag{66}$$

where we have broken the volume integral into a cross-sectional integration and an axial integration.

Equation (66) is a new source-field relationship that evaluates the extracellular field from sources arising from the propagating action potential on a single fiber in an unbounded volume conductor. Using Eq. (41) we can identify the cross-sectional integral [including the coefficient $1/(4\pi\tau_e)$] as evaluating the field of a unit magnitude double-layer disc (with the fiber radius a) oriented in the z direction. If z is the source location the result of the cross-sectional integration can be written $W_d[\rho', (z - z')]$ where (ρ', z') are the coordinates of the field point. The quantity in Eq. (66) namely $\tau(z) = \partial[\sigma_e\Phi_e(z) - \sigma_i\Phi_i(z)]/\partial z$ constitutes the double-layer (disc) density (a function of z). So, we also can write Eq. (66) as

$$\Phi_e(\rho', z') = \int_z \tau(z)W_d[\rho', (z - z')]dz \tag{67}$$

a convolution integral that can be evaluated using the fast Fourier transform (FFT). For extracellular field points, Eq. (66) identifies the source as a volume dipole distribution that fills the intracellular space of the fiber. Such a source is not a real source, it does not correctly give the intracellular field, but is an *equivalent* source. It does give the correct field for any z' and for $\rho' \geq a$, that is, for any extracellular field point.

Equation (66) can be integrated by parts, and this gives two additional expressions. (Note that, in this integration, the integrated parts go to zero because at the ends of a long fiber field quantities are all zero.) The results are

$$\Phi_e(p) = \frac{1}{4\pi\sigma_e}\int_z \frac{\partial^2}{\partial z^2}[\sigma_i\Phi_i(z) - \sigma_e\Phi_e(z)]\,dz \int_A \frac{1}{R}\,dA \qquad (68)$$

and

$$\Phi_e(p) = \frac{1}{4\pi\sigma_e}\int_z [\sigma_i\Phi_i(z) - \sigma_e\Phi_e(z)]\,dz \int_A \frac{\partial^2(1/R)}{\partial z^2}\,dA \qquad (69)$$

In Eq. (68) the cross-sectional integral is the field of a single-layer disc lying in the fiber cross section. The extracellular field is the convolution of this field with the source density function given by

$$K(z) = \frac{\partial^2}{\partial z^2}[\sigma_i\Phi_i(z) - \sigma_e\Phi_e(z)] \qquad (70)$$

The extracellular field in this formulation arises from a volume current-source density $I_v = \pi a^2 K(z)$ with $K(z)$ given in Eq. (70).

In Eq. (69) the cross-sectional integral can be identified as the field from a disc of axial quadrupoles (a single such quadrupole consists of two axial dipoles displaced in the z direction). In this formulation the function we called $\sigma_i V_f(z)$ is itself the source-density function. All the aforementioned sources are equivalent sources and all give the same answer in the extracellular region. Depending on V_f and the geometry one of these may be particularly attractive either for simplicity in calculation or for its clear physical interpretation or both. But, clearly, all formulations will give identical results.

For source-field distances that are large enough the single-layer disc in Eq. (68) can be approximated by a localization of the source on the axis. One can examine this approximation by comparing the field of the disc with that of a point source of the same total strengh at the disc origin. For $R/a \geq 5$ the error will be under 1% (13). Given this condition, we may replace

$$\int_A \frac{1}{R}\,dA = \frac{\pi a^2}{R} \qquad (71)$$

One can also show that for the unbounded volume conductor Φ_e is very small and can be neglected. (Under these conditions we can also replace Φ_i by v_m.) Assuming both approximations permits the conversion of Eq. (68) into

$$\Phi(\rho', z') = \frac{a^2\sigma_i}{4\sigma_e}\int_z \frac{1}{R}\frac{\partial^2 v_m}{\partial z^2}\,dz \qquad (72)$$

which corresponds to Eq. (31). In the derivation of Eq. (72) however, we have a clearer picture of the underlying approximations.

Multicellular Preparations—Cardiac Muscle and Bidomain

For a small bundle of muscle fibers that are approximately of similar diameter and on which an action potential is propagating from the same origin, one could apply Eq. (66), (68), or Eq. (69) to each fiber and sum their contributions to evaluate the total extracellular field. (Fortunately physiological volume conductors are linear and superposition applies.) If Φ_e at the deep fibers is small, as is true at the periphery, an assumption that would be correct only for a small bundle (see Ref. 14 for details), then the total source is distributed uniformly through the entire bundle (reduced by the usually small volume fraction occupied by source-free intercellular space). The result is similar to a single fiber with the diameter of the bundle (except that the actual action potential velocity and spatial extent is determined by a single component fiber diameter and not the bundle diameter). For thick bundles an analytic approach is needed (14), some of the groundwork for which follows.

Cardiac muscle cells may be thought of as cylindrical with a length of approximately 100 μm and a diameter of approximately 12 μm. These cells are stacked together leaving only perhaps 15% of the volume for the extracellular (interstitial) fluid. Cells are interconnected at many points with junctions that have a relatively low resistance. The connections (called *connexons*) are proteins that include an aqueous channel so that, regarding ion movement, the intracellular space of all cells are directly interconnected. Cells are organized into fibers, which, macroscopically, encircle the heart in a double spiral. If such a tissue is activated at a point, propagation spreads outward in all directions, although the velocity along the fibers will be some three times greater than across them (i.e., the wavefront will be ellipsoidal). But that propagation away from the stimulus site is relatively *uniform* (a consequence of the many intercellular junctions) gives rise to the view of cardiac tissue to be *syncytial* (continuous).

Following activation Eq. (53) can be applied to every cell to establish the distribution of cardiac sources. At each membrane there is a double-layer given by Eq. (53). Because each cell is relatively small (compared to a likely distance to field points of interest) the single net resultant dipole arising from the vector sum of the cell's double-layer elements are a good approximation to that distributed double-layer source. Furthermore, from the fact that there are perhaps 10^{10}cells in the heart, a distributed dipole volume density function (designated as $\boldsymbol{J}^i$) can be determined. In evaluating this density function at every point the contributions from a small volume is summed and divided by the volume. Ideally the volume should be very small (approaching zero), but in this case although cells are small their size cannot be ignored. So in evaluating the density function the volume should be small enough for a reasonable resolution but not so small that there are insufficient cells to obtain a satisfactory average. This is referred to as a *coarse-grain* average. We assume that the underlying physiological processes insure smooth spatial transitions so that $\boldsymbol{J}^i$ is well behaved mathematically. The field from this source is described using Eq. (41), as

$$\Phi_e = \frac{1}{4\pi\sigma}\int_V \boldsymbol{J}^i \cdot \nabla(1/R)\,dv \qquad (73)$$

(because, as noted earlier, $\nabla(1/R) = \boldsymbol{a}_R/R^2$). The volume V in Eq. (73) should include all sources, and this is assured by taking the integral over the entire heart. We now apply the following vector identity $\nabla \cdot (\phi \boldsymbol{A}) = \nabla\phi \cdot \boldsymbol{A} + \phi\nabla \cdot \boldsymbol{A}$ to the scalar vector product $(1/R)\boldsymbol{J}^i$ and get

$$\nabla \cdot (\boldsymbol{J}^i/R) = \nabla(1/R) \cdot \boldsymbol{J}^i + (1/R)\nabla \cdot \boldsymbol{J}^i \tag{74}$$

Substituting from Eq. (74) into Eq. (73) yields

$$\Phi_e = \frac{1}{4\pi\sigma}\left[\int_V \nabla \cdot (\boldsymbol{J}^i/R)\, dv - \int_V (1/R)\nabla \cdot \boldsymbol{J}^i\, dv\right] \tag{75}$$

The first integral on the right-hand side of Eq. (75) can be converted into a surface integral using the divergence theorem. Because the volume is the entire heart, this integral evaluates to zero since at the surface of the heart $\boldsymbol{J}^i = 0$. Consequently, an alternate formulation to Eq. (73) is

$$\Phi_e = -\frac{1}{4\pi\sigma}\int_V (1/R)\nabla \cdot \boldsymbol{J}^i\, dv \tag{76}$$

An examination of the form of Eq. (76) [compare with Eq. (34)] identifies $-\nabla \cdot \boldsymbol{J}^i$ as a volume source density (with previous notation we've shown that $I_v = -\nabla \cdot \boldsymbol{J}^i$).

Substituting the expression for I_v into Eq. (35) and rearranging results in

$$\nabla \cdot (\boldsymbol{J}^i - \sigma\nabla\Phi) = 0 \tag{77}$$

In Eq. (77) the vector quantity in parenthesis is solenoidal; therefore, we can identify it as the total current, $\boldsymbol{J}_t$, which has the appropriate zero divergence by virtue of the continuity of current. Consequently

$$\boldsymbol{J}_t = \boldsymbol{J}^i - \sigma\nabla\Phi \tag{78}$$

showing that the total current density is the sum of the ohmic (conduction) current, $\sigma\boldsymbol{E} = -\sigma\nabla\Phi$, plus $\boldsymbol{J}^i$. But whereas $\boldsymbol{J}^i$ was introduced as a dipole source density it now appears as an *applied current density* (both interpretations have the same dimensions, of course).

Although cardiac muscle is actually made up of a collection of discrete cells we have introduced $\boldsymbol{J}^i$ as a source function that is continuous. The same simplification can be introduced in regard to the cardiac tissue structure. The fine details of this structure include the collection of cells where each cell is connected to its neighbors by roughly ten junctional elements (15). But on a global basis the intracellular space can be regarded as a continuum. A similar argument can be applied to the interstitial space, which, although containing many convolutions on a subcellular scale, yet macroscopically may be considered through an averaged, continuous medium. Such a model is known as a *bidomain* since it consists of an intracellular and an interstitial (continuous) domain. In view of the noted preferential propagation along fiber axes (reflecting higher conductivity values in this direction) the cardiac bidomain can be expected to be anisotropic. A further simplification is to define the intracellular and interstitial domains on the same tissue space. For a given (bidomain) coordinate an intracellular and extracellular potential would be retrieved; their difference is the transmembrane potential at that point (it is actually the average over a small surrounding region), and this value is a solution to the membrane equations at that same point. That is, the membrane in the bidomain is also distributed throughout the tissue space providing a link between intracellular and interstitial domains. In summary, we give up the fine detail for the simplification of a continuous medium where continuum mathematics may be applied.

Bidomain—Mathematical Description

Possibly a more satisfactory description of the bidomain utilizes the language of mathematics. In each domain we require that Ohm's law be satisfied. Accordingly, letting i refer to intracellular and e interstitial, we get

$$\boldsymbol{J}_i = -\left(g_{ix}\frac{\partial\Phi_i}{\partial x}\boldsymbol{a}_x + g_{iy}\frac{\partial\Phi_i}{\partial y}\boldsymbol{a}_y + g_{iz}\frac{\partial\Phi_i}{\partial z}\boldsymbol{a}_z\right) \tag{79}$$

and

$$\boldsymbol{J}_e = -\left(g_{ex}\frac{\partial\Phi_e}{\partial x}\boldsymbol{a}_x + g_{ey}\frac{\partial\Phi_e}{\partial y}\boldsymbol{a}_y + g_{ez}\frac{\partial\Phi_e}{\partial z}\boldsymbol{a}_z\right) \tag{80}$$

In Eqs. (79) and (80) the conductivities are assumed to be different in each of the principle directions. For cardiac tissue normally one of the principle directions is along the fiber axis, say z (for both regions), whereas in the transverse direction we often expect $g_{ix} = g_{iy}$ and $g_{ex} = g_{ey}$ based on structural symmetry. The currents evaluated in Eqs. (79) and (80) are constrained by the continuity of current, so that whatever leaves one domain must appear in the other (except when current is introduced or removed with an electrode) and thus

$$-\nabla \cdot \boldsymbol{J}_i = \nabla \cdot \boldsymbol{J}_e = I_m \tag{81}$$

where I_m describes the transmembrane current per unit volume.

If the microscopic intracellular conductivity is σ_i and microscopic extracellular conductivity is σ_e, then the bidomain conductivities can be estimated from the tissue structure. Let us assume that there is a uniform fiber orientation in the z direction where the relative cross-sectional area occupied by the intracellular region is p, and hence that occupied by the interstitial region is $(1 - p)$. In this case we'd get

$$\begin{aligned} g_{iz} &= \sigma_i p \\ g_{ez} &= \sigma_e(1-p) \end{aligned} \tag{82}$$

Here we have taken into account that the actual relative intracellular cross-sectional area is $p < 1$, whereas in the bidomain, because the full tissue space is occupied, it is now raised to 1 and hence the bidomain conductivity must be proportionately reduced. A similar argument applies to the interstial bidomain conductivity. For the transverse directions the geometrical factor is more difficult to evaluate. For circular cylindrical fiber arrays the transverse interstitial conductivity (16) has been found to be

$$g_{ex} = g_{ey} = \frac{1-p}{1+p}\,\sigma_e \tag{83}$$

In view of the complex structure of cardiac tissue experimental determination of bidomain conductivities is normally re-

quired. However there are only two such investigations, at present, and these have significant disagreements (17,18).

Electrodes—Reciprocity

We have focused attention on the evaluation of volume conductor fields from sources in excitable tissues. If the potential field is evaluated at the surface of the body then a pair of small electrodes will sample this field and record the difference in potential. But if the electrode is large compared to spatial variations in potential then the measured potential is an averaged value. How should the average be taken? It can be shown that relative to a remote site an electrode with a conducting surface S_e lying in an (applied) potential field Φ_a (in the absence of the electrode) measures a voltage, V, (19) given by

$$V = \int_{S_e} \Phi_a J_r \, dS \tag{84}$$

where J_r is the volume conductor current density at the electrode surface S_e that arises when a unit current is put into the electrode and removed at the remote reference. This reciprocal current, J_r, behaves as a weighting function. For a spherical or circular cylindrical electrode J_r may be uniform and the weighting similarly uniform. For a surface electrode one expects an increased weighting to arise near the edges.

Another useful formulation that is helpful in considering the signals measured by an electrode comes from the application of *reciprocity*. Consider a bounded volume conductor of volume V at the surface of which are placed two recording electrodes, a and b, which yield a measured voltage V_{ab}. The source is described by a volume distribution $\boldsymbol{J}^i$ within V. The reciprocity theorem states that

$$V_{ab} = \int_V \boldsymbol{J}^i \cdot \nabla \Phi_r \, dv \tag{85}$$

where Φ_r is the potential field arising from the introduction of a unit current into electrode a and its removal from electrode b. This *reciprocal* potential field is associated with a current density $\boldsymbol{J}_r = -\sigma \nabla \Phi_r$ where σ is a conductivity function of position [i.e., Eq. (85) applies to an arbitrary *inhomogeneous* volume conductor]. In electrocardiography J_r is defined as the *lead field* of electrodes a and b, one of which may be a reference electrode. Equation (85) provides an interpretation of the measured voltage as a weighted average of the dot product of the dipole volume source density with the lead vector field ($\boldsymbol{J}_r$). One can seek to emphasize or deemphasize certain source regions or to emphasize no region (uniform sensitivity), but since Φ_r necessarily satisfies Laplace's equation there are severe limitations on what can actually be done.

The bidomain model provides a suitable basis for evaluating the aforementioned sources given intracellular and interstitial potential distributions. A mathematically well-behaved gradient during both activation and recovery within a local region (consisting of a small number of cells within which uniformity can be assumed) permits setting, based on Eq. (66),

$$\boldsymbol{J}^i = p \nabla (\sigma_e \Phi_e - \sigma_i \Phi_i) \tag{86}$$

Appropriately since $\boldsymbol{J}^i$ is an averaged dipole moment density it is derived from averaged (bidomain) fields (Φ_e, Φ_i). In Eq. (86) the volume fraction of cells, designated p, is included since the equivalent sources only lie within the cellular volume as pointed out in Eq. (66).

APPLICATIONS

This section is devoted to a presentation of four systems in which electrical signals arising from specific organs are recorded; the goal in each case is to obtain information about the sources of each signal. The aforementioned systems are the electrocardiogram (ECG), electromyogram (EMG), electroencephalogram (EEG), and electrogastrogram (EGG). Each is treated in detail as a separate chapter in this volume; the consideration here is limited solely to a discussion of source-field relationships introduced in this chapter. Our interest centers on the quantitative evaluation of sources and on pertinent aspects of the volume conductor for each of the aforementioned systems. This introduces more advanced material as well as illustrate the application of the earlier material of this chapter.

Electrocardiography

Information on the electrical activity within the heart itself comes, mainly, from canine studies where multipoint (plunge) electrodes are inserted into the heart. The instant in time that an activation wave passes a unipolar electrode is marked by a rapid change in potential (the so-called intrinsic deflection) and, based on recordings from many plunge electrodes, it is possible to construct isochronous activation surfaces. The cardiac conduction system initiates ventricular activation at many sites nearly simultaneously and this results in an initial broad front. The syncytial nature of cardiac tissue appears to result in relatively smooth, broad, activation surfaces, and because fibers lie parallel to the endocardium and epicardium the anisotropy insures wavefronts to also lie parallel to these surfaces.

The temporal cardiac action potential has a rising phase of approximately 1 msec, followed by a plateau of perhaps 100 msec and then by slow recovery, which also requires approximately 100 msec. Because activation is a propagated phenomena, a *spatial* action potential can be obtained from the temporal version since the space-time function must be of the form of a propagating wave $v_m(s - \theta t)$ where s is the local direction of propagation and θ the velocity. Thus behind the isochronal wavefront is a region undergoing depolarization (for $\theta = 50$ cm/sec and a rise time of 1 msec its thickness is 0.5 mm (it is hence quite thin and often approximated as a surface). Behind that, the tissue is uniformly in the plateau state while ahead of the activation wave it is uniformly at rest. Application of Eq. (86) shows that there are no sources except in the region undergoing activation (the gradient being zero wherever v_m is unvarying). Thus the activation source is a volume double layer with a thickness of around 0.5 mm lying behind the activation isochrone. The total strength of the double layer is given by integrating Eq. (86) in the direction of propagation; using the bidomain model this come out

$$\tau = (V_{\text{peak}} - V_{\text{rest}}) \frac{r_e}{r_i + r_e} \tag{87}$$

where r_i and r_e are bidomain intracellular and extracellular resistance per unit length in the direction of propagation and V_{peak} and V_{rest} describe the peak and resting values of the action potential. The value of τ in Eq. (87) has been found from the component potentials and resistances and also from direct measurement of the potential across an activation wave and consistent values of $\tau = 40$ mV found (20). Because the activation wave is only 0.5 mm thick the double layer may be considered to lie in the surface corresponding to the activation isochrone.

That activation sources are limited essentially to a surface is a consequence of an activation time of 1 msec. Recovery, on the other hand occupies 100–200 msec and consequently recovery sources are distributed throughout the heart. To make things even more complicated, recovery is not propagated (although cells undergoing recovery can and do influence neighboring cells). Of course Eq. (86) continues to apply, but the spatial distribution of potentials now depends on spatial variations in waveshape. Assuming that cells recover earlier at the epicardium than at the endocardium would result in equiphase surface propagation from epicardium to endocardium, and hence the dipole density found from Eq. (86) which is outward during activation is also (on average) outward during recovery (and this would account for the observed upright QRS and T waves). Although action potential morphology can be readily examined at the epicardium and endocardium (with good resolution using optical or microelectrode techniques) in vivo intramural action potential waveforms are not accessable (although aspects, like refractory period, can be sampled).

In vitro and isolated cell electrophysiology, although less reliable quantitatively (since cellular interactions are abnormal), reveal that the variation in action potential duration from endocardium to epicardium is not monotonic, as assumed above. Recent work of the Antzelevitch group (21) describes a mid-wall region containing M cells which have the longest action potential durations. Consequently the T-wave sources are more complex in distribution and orientation. While they are not uniformly outward, indeed they appear to be inward in the subendocardial region, the collective dipole source direction is outward.

In connection with recovery, interest over the years has developed in the time-integrated electrocardiogram. This can be interpreted as the algebraic area of the QRS and T waves and is consequently designated A^{QRST}. For the jth lead, with lead vector field $\boldsymbol{l}_j(v)$, it has been shown that, based on Eqs. (85) and (86) (22)

$$A_j^{QRST} = -C \int_{heart} \nabla\mu \cdot \boldsymbol{l}_j \, dv \tag{88}$$

where μ is the area of the action potential (a function of position) and the volume integral in Eq. (88) is taken throughout the heart. If the cardiac action potentials all had similar shapes but the duration of the plateau was a variable (possibly this *is* the leading difference in morphology), then

$$A_j^{QRST} = -C \int_{heart} \nabla d \cdot \boldsymbol{l}_j \, dv \tag{89}$$

where d is the action potential duration (23). The dependence of the integrated electrocardiogram on the recovery gradient, described in Eq. (89), led to its designation as the *ventricular gradient*. Dispersion of recovery has been linked to a propensity for arrhythmias; so the ventricular gradient has been examined as a possible evaluative tool.

We have concentrated most of our attention on cardiac sources, but to complete a forward simulation one must also consider the volume conductor. This is clearly inhomogeneous the most important inhomogeneity being the finite torso itself. Other components are the blood cavities, the lungs, and the surface muscle layer. The latter is anisotropic but is usually taken into account by increasing its thickness by a factor of three. Assuming that each tissue is uniform limits the secondary sources to the various interfacial surfaces. This formulation lends itself to a forward solution by the boundary element method (BEM). A number of studies have appeared in the literature mostly demonstrating inhomgenieties to be of importance, although the effect is more pronounced on the quantitative body surface potentials and less on their temporal and spatial potential patterns (24,25).

Electromyography

In electromyography the source arises from action potentials propagating in whole muscle. Muscles of greatest interest are those at the extremities. Potentials may be measured noninvasively at the body surface or minimally invasive with electrodes inserted into the muscle itself with a hypodermic needle. The latter electrodes may be macroscopic (from the uninsulated portion of the shaft of the needle), or from a small wire electrode whose tip lies within a very small hole in the needle wall (called a *side-arm*), which is useful in recording single-fiber EMGs (SFEMG). Needle electrodes are also available with multiple holes to achieve multiple leading off points that may be recorded simultaneously. In addition a single concentric electrode is also available that is sensitive to only a few fibers or possibly an SFEMG. The clinical goal is to evaluate pathologies such as atropic or hypertropic fibers or changes in fiber distribution from abnormalities in the EMG.

For the macro-EMG, as noted above, one channel is derived from the needle electrode canula (with an uninsulated tip 15 mm long). The sideport is located 7.5 mm from the tip and contains a single electrode 25 μm in diameter. This records an SFEMG. It may be used to trigger the canula signal, which when averaged over a succession of signals selects the activity of a single motor unit (that associated with the SFEMG). Accordingly the canula signal, which ordinarily reflects many motor units, may then be said to yield a macro motor unit potential (MMUP).

Simulation is a useful tool to investigate the properties of EMG signals. For the MMUP a number of factors must be considered. The motor unit contributing to the potential field are fibers activated by a single motor neuron that may actually have one or more branches introducing possible latencies between groups of inervated muscle fibers. In addition, muscle fiber endplates are dispersed resulting in a desynchronization of action potentials traveling on each fiber. A third factor contributing to a variation among the individual fibers in a motor unit is their difference in fiber diameter (and hence in velocity which is usually assumed to be linearly proportional). Finally there is the effect of fiber geometry within the motor unit (the fiber density is not uniform) and the relative location of the recording electrode.

Nandedkar and Stålberg (26) has suggested the use of a line source model, such as described by Eq. (72). If we assume that symmetry is axial the weighting function in cylindrical coordinates is given as

$$W_s(\rho' z') = \frac{1}{4\pi\sigma_\rho \sqrt{K\rho'^2 + (z - z')^2}} \tag{90}$$

where $K = \sigma_z/\sigma_r$. This result differs from $1/R$ in Eq. (33) because it is assumed that a single fiber in a muscle bundle lies in an anisotropic monodomain medium, which can be described by the radial, axial conductivity parameters σ_r, σ_z. A further weighting arises from the large canula surface area, and this necessitates a surface integration of Eq. (90) of the type shown in Eq. (84), the result of which we designate W_S. (As an approximation the canula may be considered uniform and its surface integral estimated from a line integral giving a simple average). The potential function is given by

$$\Phi_e = i_m(z) * W_S \tag{91}$$

where $*$ denotes convolution and $i_m = \sigma_i \pi a^2 \partial^2 \Phi_i / \partial z^2$.

Because there are many active fibers in electromyography it is of particular interest to know the extent of the sensitivity of a particular electrode when inserted into the muscle. This is designated the *pickup area.* It may be examined through the application of reciprocity and a description of the lead field, as pointed out with Eq. (85).

For simulations of the EMG at the surface of a limb the volume conductor comes into consideration. To date this has been assumed to be uniform in conductivity and only the boundary with air interface acknowledged. The simplest model is one that assumes the bounding tissue–air interface to be semiinfinite in extent. This permits a consideration of the contribution of the secondary sources by the method of images. A better approximation is to treat the limb as circular cylindrical. Simulations using the latter model demonstrate the shortcomings of the former, particularly for deep fibers (27).

Electroencephalography

The electrical activity of the brain can be detected using scalp electrodes; its *spontaneous* sources generate the electroencephalogram (EEG). Such sources arise from a large number of cells. However, in contrast with the ECG and EMG, the EEG apparently does not significantly involve action potentials of neuronal cells but rather is associated with the synaptic activity that precedes or follows activation. Actually EEG sources are believed to arise mainly from postsynaptic potentials (PSP) on cortical pyramidal cells. A large number of cells appear to underlie a detectable signal, and this implies temporal (and spatial) synchronization. If invasive intracellar recording is undertaken, both spike (action potential) and wave type activity is found; abolition of the latter terminates the EEG. In addition to the aforementioned spontaneous activity giving rise to the EEG as measured at the scalp, one can also obtain signals that are a response to stimuli using auditory, visual, and tactile modalities. These are described as *evoked potentials.*

As we learned from Eq. (86), a region consisting of excitable cells will establish an electrical source provided that a gradient of transmembrane potential exists. For nerve cells this occurs when an action potential has been elicited and also when synaptic potentials are developed. In addition transmembrane potentials can also arise from the passive flow of current across membranes (as is expected in cardiac and skeletal muscle tissue). The effect of this factor may instead be approximated by including the passive membrane in an averaged specification of the volume conductor impedance (e.g., by defining an appropriate anisotropic bidomain).

The response to sensory stimulation and some types of pathology is a region of cellular activity that often is circumscribed (*focal*). In this case we may assume that the source (were it in an unbounded region) would generate the field, based on Eq. (59), given by

$$\Phi = \frac{1}{4\pi\sigma} \frac{\boldsymbol{a}_R}{R^2} \cdot \left[\sum_j \int_j (\sigma_e \Phi_e - \sigma_i \Phi_i)\, d\boldsymbol{S}_j \right] \tag{92}$$

requiring a summation over all cells S_j. Equation (92) neglects the distribution of cellular sources, an approximation that improves as the region diminishes in size. Defining a continuous volume dipole source function, $\boldsymbol{J}^i$, as was done leading to Eq. (73), permits the simplification of Eq. (92) into

$$\Phi = \frac{1}{4\pi\sigma} \frac{\boldsymbol{a}_R}{R^2} \cdot \left(\int_V \boldsymbol{J}^i\, dv \right) \tag{93}$$

In order that $\boldsymbol{J}^i$ not average out to zero, synchronization of sorts appears to be required. The result, according to Eq. (93), is a single focal dipole source. A number of articles have been directed to determining such a source (its magnitude, direction, and location) (28).

Whether or not the dipole density distribution can be considered to approximate a single dipole, the measured surface voltage can be interpreted with the application of reciprocity. According to Eq. (85) a distributed source $\boldsymbol{J}^i$ contributes to the lead voltage V_{ab} according to

$$V_{ab} = \int_V \boldsymbol{J}^i \cdot \nabla \Phi_r\, dv \tag{85}$$

In the present context included in $\boldsymbol{J}^i$ are the neuronal sources arising from action potentials as well as synaptic potentials. The reciprocal field must, at a minimum, include the influence of the brain tissue, the skull, and the scalp. In view of the large differences in conductivity the reciprocal field actually available at brain sources is quite different from what would arise were aforementioned regions homogeneous. If the skull resistivity is taken as 80 times that of the brain and scalp, then the lead field is diminished 20-fold (a measure of the shunting effect of the scalp-skull) based on a concentric spheres volume-conductor model (29).

Electrogastrography

Electrogastrography (EGG) refers to the measurement of electrical signals at the surface of the abdomen whose sources lie in the smooth muscle of the stomach. The system is thus basically the same as in the previous applications. Internal gastric electrical activity (GEA) have also been investigated, but because such measurements are truly invasive there is only limited human data. However even these measurements are

macroscopic; intracellular data is even harder to obtain. As a consequence, what is available about the electrical activity of the smooth muscle is inadequate for a quantitative evaluation of sources, such as described for the EMG and ECG. In its place are empirical dipole source models, which are then combined with a volume conductor model.

The stomach is bean-shaped with food entering from the esophagus at the top passing through the fundus and body regions into the lower region (the antrum), from which it then passes through the pylorus and enters the duodenum (small intestine). The stomach is lined with a longitudinal muscle layer at the outside and within which is a circular muscle layer. Electrical activity starts at a pacemaker region somewhat near the fundus and travels distally via the longitudinal muscle. Activity spreads inward from the longitudinal muscle through the thicker circular muscle. A background electrical activity (electrical control activity, ECA) is always present; a second component, which it may trigger, is the electrical response activity (ERA). The ERA is associated with contractions and spiking (action potentials). Because it is noninvasive, the EGG is of interest in gastroenterology, but the signal is low (100–500 mV) and must be separated from other bioelectric signals and noise (motion and respiration sources).

The EGG does not present a recognizable morphology, as with the ECG, and tends to be quite noisy. Accordingly the clinical approach is to evaluate only three parameters, namely amplitude, frequency, and time duration. The use of the FFT provides a useful measure of the signal frequency and this can be implemented with a running window to provide a view of the spectrum as a function of time. (The slow wave noted above shows a frequency of around 3 cycles/min.) The EGG has been examined for a determination of gastric motility, but surface recordings of such activity have proven unreliable (such information can be found with electrodes placed directly on the stomach yielding gastric electrical signals). In fact the recent study by Mintchev and Bowes (30) concludes that only the frequency dynamics forms the basis for quantitation.

There are few biophysical models of the EGG and what is available is ad hoc. The most recent of these is due to Mintchev and Bowles (31). The human stomach is represented as a truncated conoid. The sources are assumed to be an annular double layer with a width that is relatively narrow (around 2–3 mm) and with a dipole orientation normal to the surface. Sources, as such, outside this band are assumed to have random orientations and to generate no net field. The source-field equation of Mintchev and Bowles (31) is given as

$$V_Q = 1/(4\pi\epsilon) \int_S [(\boldsymbol{D} \cdot \boldsymbol{\rho})/\rho^3]\, dS \tag{94}$$

where $\boldsymbol{D}$ is the doublelayer. Equation (94) is equivalent to Eq. (73). The ECA is generated by the distal movement of the double-layer band where the velocity along the greater and lesser stomach curvatures are considered to be different. The ERA is assumed to have no influence on the model or the ECA pattern. Their model gave good predictibility, particularly on the effect of electrode position, reflecting volume-conductor influence, although no effect of inhomogeneity is included in the model.

BIBLIOGRAPHY

1. B. Hille, *Ionic Channels of Excitable Membranes.* 2nd ed., Sunderland, MA: Sinauer Assoc., 1992.
2. A. L. Hodgkin and A. F. Huxley, A quantitative description of membrane current and its application to conduction and excitation in nerve, *J. Physiol.,* **117**: 500–544, 1952.
3. D. E. Goldman, Potential, impedance, and rectification in membranes, *J. Gen. Physiol.,* **27**: 37–60, 1943.
4. A. L. Hodgkin and B. Katz, The effect of sodium ions on the electrical activity of the giant axon of the squid, *J. Physiol.,* **108**: 37–77, 1949.
5. A. Einstein, Über die von der molekularkinetischen theorie die wärme gefordertebewegung von in ruhenden flüssigkeiten suspendierten teilchen, *Ann. Physik,* **17**: 549–560, 1905.
6. E. Neher and B. Sakmann, The patch clamp technique, *Sci. Am.,* **266**: 28–35, 1992.
7. J. E. Randall, *Microcomputers and Physiological Simulation.* 2nd ed, New York: Raven Press, 1987.
8. J. Dempster, *Computer Analysis of Electrophysiological Signals.* London: Academic Press, 1993.
9. B. Frankenhaeuser, Quantitative description of sodium currents in myelinated nerve fibers of *Xenopus laevis. J. Physiol.* **151**: 491–501, 1960.
10. C-H. Luo and Y. Rudy, A dynamic model of the cardiac ventricular action potential, *Circ. Res.,* **74**: 1071–1096, 1994.
11. R. Plonsey and D. B. Heppner, Considerations of quasistationarity in electrophysiological systems, *Bull. Math. Biophys.,* **29**: 657–664, 1967.
12. R. Plonsey, The formulation of bioelectric source-field relationships in terms of surface discontinuities, *J. Franklin Inst.,* **297**: 317–324, 1974.
13. R. Plonsey, The active fiber in a volume conductor, *IEEE Trans. Biomed. Eng.* **BME-21**: 371–381, 1974.
14. C. S. Henriquez, N. Trayanova, and R. Plonsey, Potential and current distributions in a cylindrical bundle of cardiac tissue, *Biophys. J.,* **53**: 907–918, 1988.
15. R. H. Hoyt, M. L. Cohen, and J. E. Saffitz, Distribution and three-dimensional structure of intercellular junctions in canine myocardium, *Circ. Res.,* **64**: 563–574, 1989.
16. B. J. Roth and F. L. Gielen, A comparison of two models for calculating the electrical potential in skeletal muscle, *Ann. Biomed. Eng.,* **15**: 591–602, 1987.
17. L. Clerc, Directional differences of impulse spread in trabecular muscle from mammalian heart, *J. Physiol.,* **255**: 335–346, 1976.
18. D. E. Roberts and A. M. Scher, Effect of tissue anisotropy on extracellular potential fields in canine myocardium in situ, *Circ Res,* **50**: 342–351, 1982.
19. R. Plonsey, Dependence of scalar potential measurements on electrode geometry, *Rev. Scientific Instrum.,* **36**: 1034–1036, 1965.
20. R. Plonsey and A. van Oosterom, Implications of macroscopic source strength on cardiac cellular activation models, *J. Electrocard.,* **24**: 99–112, 1991.
21. D. W. Liu, G. A. Ginant, and C. Antzelevitch, Ionic basis for electrophysiological distinctions among epicardial midmyocardial, and endocardial myocytes from the free wall of the canine left ventricle, *Circ. Res.,* **72**: 671–687, 1993.
22. D. B. Geselowitz, The ventricular gradient revisited: Relation to the area under the action potential, *IEEE Trans. Biomed. Eng.,* **BME-30**: 76, 1983.
23. R. Plonsey, Recovery of cardiac activity—the T-wave and ventricular gradient. In J. Liebman, R. Plonsey, and Y. Rudy (eds.), *Pediatric and Fundamental Electrocardiography.* Boston: Martinus Nijhoff, 1987.

24. R. M. Gulrajani, F. A. Roberge, and G. E. Mailloux, The forward problem of electrocardiography. In P. W. Macfarlane and T. D. Lawrie (eds.), *Comprehensive Electrocardiology.* New York: Pergamon Press, 1989.
25. Y. Rudy, R. Plonsey, and J. Liebman, The effects of variations in conductivity and geometrical parameters on the electrocardiogram using an eccentric spheres model, *Circ Res.,* **44**: 104–111, 1979.
26. S. Nandedkar and E. Stålberg , Simulation of macro EMG unit potentials, *Electroenceph. Clin. Neurophys.,* **56**: 52–62, 1983.
27. S. Xiao, K. C. McGill, and V. R. Hentz, Action potentials of curved nerves in finite limbs, *IEEE Trans. Biomed. Eng.,* **BME-42**: 599–607, 1995.
28. J. C. De Munck, B. W. van Dijk, and H. Spekreijse, Mathematical dipoles are adequate to describe realistic generators of human brain activity, *IEEE Trans. Biomed. Eng.,* **BME-35**: 960–966, 1988.
29. S. Rush and D. A. Driscoll, EEG-electrode sensitivity—an application of reciprocity, *IEEE Trans. Biomed. Eng.,* **BME-16**: 15–22, 1969.
30. M. P. Mintchev and K. L. Bowes, Extracting quantitative information from digital electrogastrograms, *Med. Biol. Eng. Comput.,* **34**: 244–248, 1996.
31. M. P. Mintchev and K. L. Bowes, Conoidal dipole model of electric field produced by the human stomach, *Med. Biol. Eng. Comput.,* **33**: 179–184, 1995.

Reading List

R. Plonsey and R. C. Barr, *Bioelectricity: A Quantitative Approach.* New York: Plenum Press, 1988.

J. Malmivuo and R. Plonsey, *Bioelectromagnetism.* New York: Oxford Press, 1995.

D. Junge, *Nerve and Muscle Excitation.* 3rd ed., Sunderland, MA: Sinauer Assoc., 1992.

T. F. Weiss, *Cellular Biophysics.* Cambridge, MA: MIT Press, 1996.

R. D. Keynes and D. J. Aidley, *Nerve and Muscle.* Cambridge: Cambridge University Press, 1981.

F. Rattay, *Electrical Nerve Stimulation.* Vienna: Springer-Verlag, 1990.

C. A. Brebbia and J. Dominguez, *Boundary Elements.* New York: second edition, McGraw-Hill, 1992.

ROBERT PLONSEY
Duke University

BIOELECTRONICS. See MOLECULAR ELECTRONICS AND HYBRID COMPUTERS.

BIOENGINEERING. See BIOMEDICAL ENGINEERING.